Analysis of high-speed combustion regimes of hydrogen jet in supersonic vitiated airstream

Arnaud Mura, Anthony Techer, Guillaume Lehnasch

Analysis of high-speed combustion regimes of hydrogen jet in supersonic vitiated airstream

Arnaud Mura[a,*], Anthony Techer[a], Guillaume Lehnasch[a]

[a] *PPRIME UPR3346 CNRS, ENSMA and University of Poitiers, France*

Abstract

Highly-resolved reactive simulations of a hydrogen jet injected into a transverse supersonic flow of vitiated air at Mach 2 are conducted. The operating conditions are chosen to be relevant of scramjet operative conditions and are representative of experiments conducted at ONERA Palaiseau Research Center. Hydrogen injection in the supersonic vitiated airstream leads to the formation of a bow shock, which interacts with the boundary layer and gives rise to separation zones. In the resulting recirculation zones, only small amounts of OH radicals are produced. Combustion stabilization and development take place further downstream. Heat release is significant in the vicinity of the wall within a sonic region where the equivalence ratio is around two. Farther from walls, combustion takes place at supersonic speeds but features lower levels of heat release rates. Supersonic turbulent combustion regimes are analyzed in detail: first in a standard set of coordinates $(u'/S_L^0, L_t/\delta_L^0)$ using data collected in regions featuring a sufficiently large degree of premixing. Then, they are analyzed in the turbulent Reynolds and Damköhler numbers sub-space (Re_t , Da). In this representation, three distinct Damköhler number definitions based on *(i)* production rate of H_2O, *(ii)* flame propagation characteristic time, and *(iii)* ignition delay time are considered. These various representations put into evidence turbulent combustion regimes featuring significant finite-rate chemical kinetics effects. The whole set of computational results confirms that *(i)* the use of models based on the fast chemistry hypothesis is questionable for such conditions, *(ii)* taking into account finite-rate chemistry effects is essential, and *(iii)* ignition processes play a key role in combustion stabilization. The manuscript ends with some perspectives and challenging issues for future works.

Keywords: high-speed flows, supersonic combustion regimes, jet in

*Corresponding author (arnaud.mura@ensma.fr).

supersonic crossflow, turbulent combustion, finite-rate chemistry, hydrogen combustion

1. General introduction

The contribution of K. N. C. Bray to combustion science has laid the foundations for the turbulent premixed flame theory [1–23]. Indeed, his outstanding input into the mathematical description of turbulent premixed flames in the thin flame limit [1–8] has provided a solid and seminal basis for most of the fundamental research studies conducted in the field [24–33] and it remains today's cornestone of current research works devoted to the analysis and modelling of turbulent premixed combustion [34–41].

Thus K.N.C. Bray has been one amongst the pioneers in the use of statistical approaches to describe turbulent reacting flows. From the combined use of probability density functions (PDF), intermittency theory, and asymptotics [6], the fundamental and underlying physical mechanisms were identified. A typical (and remarkable) example is provided by Bray's early derivation of the relationship between the mean chemical rate and mean scalar dissipation rate (SDR) of reactive species [4], a quantity that is indeed central to a wide range of turbulent combustion closures for premixed and partially premixed conditions, *e.g.*, [29, 42–50]. Complete sets of second-order turbulence models have been also proposed so as to take the influence of thermal expansion into account. Their early developments lead to *(i)* the identification of the so-called flame-generated turbulence (FGT) production and counter-gradient diffusion (CGD) or non-gradient diffusion phenomena [7, 8] and *(ii)* the detailed analyses of the role played by pressure terms, *i.e.*, correlations between the pressure fluctuations and velocity (or composition) gradients, under the influence of local flamelet contributions [21]. With all these developments and seminal findings, K.N.C. Bray has provided solid bases for the development of flamelet methods, which offer a robust framework for the modelling of turbulent combustion [11].

In fact the contribution of K.N.C. Bray to turbulent premixed combustion is so significant that this has somehow hidden some of his other pieces of work in the field of chemical physics, ionized multicomponent mixtures and plasmas, gas dynamics, and high-speed flows in general [51–57].

From a general viewpoint, combustion in high-speed (supersonic) flows is relevant to security and safety issues, atmospheric re-entry flows, astrophysics [58], hypersonic propulsion systems [59], rocket engines and igniters, such as the one considered in reference [60]. As regards its appli-

cation to propulsion, one of the most typical examples is the scramjet engine [59, 61, 62]. For flight Mach number values larger than five (hypersonic flight), attention has been indeed early focused in the late fifties on the possibility of performing the combustion at supersonic speed so as to avoid the prejudicial effects of dissociation on combustion efficiency. Supersonic combustion was proven to be possible as early as 1962 at the Aerodynamics Laboratory of the Polytechnics Institute of Brooklyn (PIBAL) where, almost 50 years ago, combustion was stabilized in the supersonic coflowing streams geometry, see Ferri, Libby, and Sakkay [63].

In this respect, the early contribution of K.N.C. Bray to combustion in high-speed flow conditions — a challenging combustion regime that, for many years, has concentrated significant research efforts — has settled some of the bases of turbulent reactive flow modelling in these extreme conditions. The description of turbulent combustion in supersonic flows has been central to a reference book chapter written by K.N.C. Bray, P.A. Libby, and F.A. Williams [64]. The topic has been also covered by P.A. Libby in reference [65].

In comparison with their low-speed counterparts, reactive high-speed flows indeed raise some specific issues. For instance, these reactive high-speed flows do involve some special couplings between chemical reactions and compressibility effects, *i.e.*, compression waves and rarefaction waves. This is because the gas temperature is sensitive to these compression/rarefaction waves. Thus, there is a permanent exchange between internal energy (molecular scale) and kinetic energy (macroscopic scale). In this respect, it does not seem useless to remind here that the Mach number Ma is the squared root of the ratio between the kinetic energy (of the flow) and thermal energy or static enthalpy, *i.e.*, the average kinetic energy of molecules. In the vicinity of sonic conditions ($\mathrm{Ma} = 1$), the kinetic energy is indeed already of the same order of magnitude as the static enthalpy per unit mass and it becomes the main contribution as the Mach number value is increased beyond unity. Therefore, since the kinetic energy dissipation induced by molecular viscosity effects, in boundary layers, shear layers or shock waves, is proportional to the squared Mach number Ma^2, moderate changes in velocity result in non-negligible changes in static temperature and pressure. Considering the sensitivity of chemical reactions to temperature and pressure, this induces a coupling between the velocity field and chemical reactions. The consideration of these effects therefore appears as one amongst the specific challenges of high-speed turbulent combustion modelling and the early works of Bray and his coworkers [66, 67] has served as a basis to some of the seldom modelling proposals that attempted to address this issue [68–72]. In this respect,

the early developments made in references [66–68] were conducted within the laminar flamelet framework and this raises the question of the combustion regimes [73, 74] relevant to such conditions. This specific — and still open question — that has seldom been addressed [75–77] since the work of Balakrishnan and Williams [75] is central to the present study.

The manuscript is organized as follows: the next section (Sec. 2) provides a brief overview of the computational database that is used to proceed with the present investigation ; it is followed by a short section (Sec. 3) where some features of the unburnt mixture (temperature and reactivity) are scrutinized. The analysis of high-speed combustion regimes, which is the core of the present study, is detailed in Sec. 4. Finally, perspectives for future works are gathered in a conclusion section that ends the manuscript.

Table 1: Main characteristics of the computational grid. The lengths and mesh sizes are normalized by D, the diameter of the injector.

direction	x	y	z
length	190.0	8.85	20.0
number of points N_{x_i}	2253	196	193
stretching factor (%)	0.35 to 0.55	2.0 to 3.0	1.70 to 3.15
mesh sizes	0.03 to 0.10	0.003 to 0.250	0.03 to 0.30

2. Overview of the computational setup and database

The present analysis is based on highly-resolved numerical simulations databases obtained with the massively parallel solver CREAMS. It solves the three-dimensional unsteady compressible Navier–Stokes equations for multi-component reactive mixtures by combining high-order spatial discretization schemes (7th order WENO and 8th order centered) with a 3rd order time integration. Its capabilities have been previously assessed through many computational investigations devoted to high-speed flows [60, 72, 78–87]. The details of the mathematical model and numerical methods used in the solver are not reported here, just for the sake of conciseness, and can be found together with an extensive verification and validation of the computational solver in references [88, 89]. The set of transport equations that has been solved can be found in reference [81]. Finally, it must be precised that the present computation has been conducted using a modified version of the Hirschfelder and Curtiss approximation to evaluate mass diffusion coefficients [90].

Table 2: Hydrogen jet and vitiated air inlet boundary conditions [91].

	hydrogen jet	vitiated airstream
ξ (-)	1.0	0.0
Y_{H_2} (-)	1.0	0.0
Y_{O_2} (-)	0.0	0.2527
Y_{H_2O} (-)	0.0	0.1631
Y_{N_2} (-)	0.0	0.5842
p / p_0 (Pa / Pa)	502,918 / 958,055	56000 / 409000
T / T_0 (K / K)	248 / 300	1108 / 1695
ρ (kg·m^{-3})	0.490	0.161
γ (-)	1.42	1.27
Ma (-)	1.0	2.0
u (m·s^{-1})	1204	1313
m (g·s^{-1})	1.85	146.55

The configuration corresponds to the three-dimensional simulation of a sonic hydrogen jet issuing from a flat plate into a Mach 2 vitiated air crossflow. Such a geometry is well-known and often referred to as a jet in supersonic crossflow (JISCF). It is sketched in Fig. 1. The conditions are representative of those considered in the dual mode ramjet investigations conducted on the LAPCAT-II setup in the ONERA-LAERTE facility [91–93]. In the present study, the computational domain is reduced to a restricted part of the experimental setup: it corresponds to the full width and half-height of the real combustion chamber and the computation meets the inlets flow conditions (*i.e.*, those associated to the hydrogen and vitiated air streams) in terms of velocity, pressure, composition, and temperature. Since the computed geometry is only half of the height of the real geometry and since an extrapolation boundary condition (BC) is specified at the top of the computational domain[1], there is no possible shock wave reflection, which is a significant difference between the retained computational geometry and the real LAPCAT-II combustor. In addition to this, it is noteworthy that some computations of the LAPCAT-II combustor model have been shown to exhibit some sensitivity to wall roughness and heat transfer modelling. One may expect that the consideration of these two effects, which is outside the scope of the present study, may influence the computational results. In this

[1]Further detail about the BC specification is provided below.

regard, according to the recent study of Pelletier *et al.* [93], it may affect the location of the combustion stabilization region.

The dimensions of the corresponding domain together with the main characteristics of the computational grid are reported in Table 1. The corresponding cartesian grid is depicted in Fig. 2. The quantity x denotes the streamwise coordinate, y is the wall-normal coordinate, and z is the spanwise coordinate. The quality of the computational grid has been assessed by using the detailed procedure described in reference [86], which has been introduced to analyze mesh reliability. The corresponding procedure combines several verification subsets including *(i)* the inspection of distributions of wall mesh sizes, *(ii)* the analysis of normalized velocity profiles in boundary layers, and *(iii)* the verification of some mesh quality indexes distributions [94, 95]. In this respect, it has been found that ninety-nine percent of the computational cells feature a value of the Pope's quality index IQ_k that is larger than 0.92. At this level, it seems also worth precising that the present highly-resolved large-eddy simulation has been conducted with the WALE sub-grid scale (SGS) viscosity model and the mesh quality has been also analyzed through the inspection of viscosity ratio profiles and wall-normalized velocity profiles as previously reported by Techer *et al.* [81] and Ribeiro *et al.* [86]. They are not included here just for the sake of conciseness. As regard chemical reactions, no sub-grid turbulent combustion model has been used, on the grounds that, in the region of interest for this study — where the heat release rate (HRR) is significant — the resolved scales control the combustion processes. Indeed, in the vicinity of the wall — where combustion develops — the flow (*i.e.*, velocity) field resolution requirement itself is very constraining. In this respect, SGS-based Damköhler number values were evaluated from various definitions based on either the fuel consumption rate or on the overall production/destruction rates of intermediate species such as hydrogen atom H or hydroperoxyl radical HO_2. Their values were systematically found to be smaller than unity. Ror instance, based on the hydroperoxyl radical HO_2, more than ninety-nine percent of the values obtained for $\mathrm{Da}_{\mathrm{sgs}} = \tau_{\mathrm{sgs}}/\tau_{\mathrm{HO_2}}$ are smaller than 0.1 and, according to the literature, see for instance Bouheraoua *et al.* [96], values of $\mathrm{Da}_{\mathrm{sgs}}$ smaller than unity also reflects — to some extent — the quality of the computational resolution. From all the information that has been gathered, it seems that the present computation is indeed a highly-resolved LES that is approaching DNS resolution requirements in the region where the HRR becomes significant. As a consequence, the notation retained for any filtered quantity $\widetilde{q}$ will not be discriminated from its instantaneous counterpart q. Thus, the filtered value will be hereafter denoted by q just for the sake of simplicity.

In this respect, it is also noteworthy that the averaged value will be denoted by $\langle q \rangle$, while its Favre-averaged counterpart will be denoted by $\{q\}$.

The computational domain extends from $-40.0\,D$ upstream to $150.0\,D$ downstream of the fuel injector exit along the streamwise direction, with D being the diameter of the injector, see Fig. 1 and Fig. 2. Along the spanwise and wall normal directions, the domain extends over $20.0\,D$ and $8.85\,D$, respectively. The sonic jet of pure hydrogen is vertically injected through an orifice of diameter $D = 2.0$ mm. The jet exit conditions correspond to a value of the jet-to-freestream momentum flux ratio $J = (\rho u^2)_{jet}/(\rho u^2)_\infty$[2] that is approximately 2.44 and to a nozzle pressure ratio (NPR $= p_{0,jet}/p_\infty$) approximately equal to seventeen. The boundary layer thickness is equal to $1.1\,D$ at the inlet of the computational domain (*i.e.*, $x/D = -40.0$). The center of the injection port is located in the middle of the bottom plane, *i.e.*, (0.0,0.0,L_z/2.0).

Taking advantage of the results issued from a preliminary RANS[3] computation of the same geometry [91], the components of the filtered velocity field at the vitiated air inlet are settled from the corresponding computed profiles of the mean velocity components. The value of the boundary layer thickness reported above has been also determined from this computation. The results of the corresponding RANS simulation could have been used to account for velocity fluctuations within the framework of synthetic inlet turbulence generators. However, some previous analyses devoted to synthetic inlet turbulence have showed that, even with properly set mean velocity and turbulence kinetic energy, the simulated flow fields are quite sensitive to the arbitrary choice of the synthetic turbulence model (*e.g.*, Digital Filter, Random Flow Generator, Synthetic Eddy Model), see for instance [97]. Another strategy may consist in running a concurrent supersonic turbulent boundary layer (STBL) simulation, making use of rescaling and reintroduction procedures, with the inflow conditions for the main simulation extracted from a plane of the concurrent STBL simulation. The associated computational costs are however non-negligible. Thus, no special effort has been spent to represent the unsteady (*i.e.*, turbulent) features of the supersonic boundary layer. This choice can be justified (at least partly) on the basis of previous reactive LES conducted on JISCF geometry, which were found able to reproduce satisfactorily experimental trends and results without taking inlet velocity fluctuations into account [98, 99]. In any case, it seems worth em-

[2]Here, the quantity u denotes the norm of the velocity vector.

[3]RANS: Reynolds-averaged Navier-Stokes

phasizing that inlet turbulence is completely altered by the wall injection, the resulting bow shock formation and associated flow separation. Moreover, we will see that the present flow conditions lead to a combustion stabilization region located quite far downstream of the upstream injection zone. The turbulence in this region is thus more likely to be driven by the development of the wake structure (downstream of the JISCF) than by the small scale structures of the turbulent boundary layer (upstream of the injection). Therefore, for the purpose of the present study, we follow a strategy similar to the one previously described by Techer *et al.* [81] and a simpler natural development of the turbulent flowfield has been chosen with no fluctuation imposed at the inlet boundary. In regard to the fuel injection, the velocity profile is set with an error function so as to mimic the presence of boundary layers. At the corresponding inlet, the mesh is generated in order to maintain approximately 50 points inside the injection diameter with at least five points within the shear layer. No-slip adiabatic wall conditions are used around the fuel injection at the bottom of the computational domain. So as to avoid any spurious numerical wave reflections, extrapolation conditions are used in conjunction with grid coarsening at the top, backside, and frontside of the computational domain. Extrapolation rules are applied at the supersonic outlet (*i.e.*, right boundary of the computational domain). Finally, the flow is initialized with the supersonic air inflow conditions in the whole computational domain. The main characteristics of the two inlet streams are gathered in Table 2. The Courant-Friedrichs-Lewy (CFL) number was adjusted between 0.9 and 1.2. Furthermore, in order to investigate the mixing between the hydrogen jet and vitiated air crossflow, we consider a fuel inlet tracer or mixture fraction (*i.e.*, a passive scalar ξ), the value of which is set to zero at the vitiated air inlet and to unity in the hydrogen jet.

The simulation is first conducted in non-reactive conditions from $t = 0.0$ until $t = t_i = 150.0\, D/u_\infty$, once the computed flowfield displays a stabilized compressible flow structure. Then, chemical source terms are activated. Combustion chemistry is described using the four-step reduced kinetic scheme of Boivin *et al.* [100], which features six reactive chemical species (H_2, O_2, H_2O, H, HO_2, and H_2O_2) and two additional chemical species (O and OH) that are evaluated from the quasi-steady-state approximation (QSSA). This reduced mechanism has been tested and validated in many elementary test cases [100]. The physical time of the simulation in reactive conditions is about $170.0\, D/u_\infty = 260.0\ \mu s$ and, over this period of time, 2250 snapshots are recorded every $0.115\ \mu s$, thus capturing the development of ignition processes and combustion stabilization.

The OH radical molar fractions obtained at three distinct times from

$t^* = u_\infty(t - t_i)/D = 80.0$ to $t^* = 170.0$ are displayed in the mid plane along the spanwise direction (see Fig. 3) and in the plane $y/D = 0.25$ along the vertical direction (see Fig. 4). From $t^* = 0.0$ to $t^* = 80.0$, the stabilization location is continuously progressing upstream (*i.e.*, towards the hydrogen injection port). Then, from $t^* = 100.0$ to $t^* = 170.0$, as illustrated in Figs. 3 and 4, the leading reactive zone (*i.e.*, the stabilization region) is observed to move back and forth between $x/D = 25.0$ and $x/D = 40.0$. The resulting averaged fields — not included due to restriction lengths — exhibit a satisfactory level of convergence.

The obtained results also show that the amounts of OH radical present in the recirculation zone upstream of the jet, which is formed just downstream of the bow shock, remain quite small, suggesting that this zone is only weakly reactive. This is in contrast with the levels of OH concentrations obtained in the wake of the jet in the near wall region, which is highly reactive. The corresponding reaction zone spreads over a region that is delineated by $z/D = -5.0$ and $z/D = 5.0$, it is however not confined in height and extends beyond the limits of the computational domain. Finally, the most significant levels of heat release rate are obtained in the vicinity of the wall within a sonic region where the equivalence ratio is around two, as it is shown in Fig. 5.

3. Preliminary analysis of the non-reactive flowfield

All the results reported in this section have been obtained from the analysis and post-processing of the non-reactive flowfield computation.

In a first step of the analysis, we proceed with the characterization of the unburnt mixture temperature which is essential since it will allow to identify the regions that are prone to the development of ignition processes. In this respect, Gamba and Mungal [101] showed that combustion stabilization in JISCF may take place in various regions of the flow: either upstream or downstream of the injector port, within the mixing layer, and further downstream, in the near-wall region, where chemical reactions were found to be the most significant. Therefore, special attention must be paid to the evaluation of the composition of the mixture (temperature and species mass fractions) in the vicinity of the walls.

Figure 6 displays scatterplots of the temperature plotted versus the mixture fraction. In the same picture is also depicted the linear approximation of the temperature evolution, *i.e.*, $T_\mathrm{u}(\xi) = \xi T_\mathrm{fuel} + (1.0 - \xi) T_\mathrm{ox}$, with the couple of values $(T_\mathrm{fuel}, T_\mathrm{ox})$ associated to the inlet stream conditions $(T_\mathrm{jet}, T_\infty)$, and with ξ the mixture fraction (or fuel inlet tracer). The data significantly

depart from the linear approximation and the variations of thermal capacities with temperature are sufficient to explain such departures. Indeed, once plotted versus the mixture fraction, the quantity that could be expected to display such a linear behaviour is the enthalpy or, more precisely, for high-speed flows such as the one considered herein, it is the total enthalpy [67, 69]. In this respect, the hydrogen jet ($\xi = 1.0$) undergoes a very high expansion and its temperature first significantly decreases. It is subsequently increased as a consequence of the Mach disk compression. The vitiated air stream ($\xi = 0.0$) is compressed through the bow shock and its temperature is further increased by viscous dissipation in the direct vicinity of the wall ($y/D = 0.0$). We will see that it is quite useful to establish a generalized (*i.e.*, non-linear) but approximated expression that relates the fresh reactants temperature to the mixture fraction. For this purpose, a sixth-order polynomial interpolation is considered: $T_{\mathrm{u}}(\xi) = a_0 + a_1\xi + a_2\xi^2 + a_3\xi^3 + a_4\xi^4 + a_5\xi^5 + a_6\xi^6$ where the quantities a_k ($k = 1, \cdots, 6$) denote the polynomial coefficients (in K). This expression will be used hereafter so as to evaluate some characteristics (*e.g.*, ignition delay and flame propagation velocity) of the unburnt mixture.

A preliminary analysis of the ignition processes is first conducted on the basis of the reactivity λ introduced by Boivin *et al.* [103, 104]. The quantity λ is the real positive eigenvalue of the Jacobian that characterizes the differential system describing the changes in concentrations of H, O, and OH. According to its definition, it is inversely proportional to the ignition delay of a homogeneous mixture. More precisely, as shown in Fig. 7, the ignition delay is of the order of $(0.06\lambda)^{-1}$ and can be readily estimated from the values of the temperature, pressure, and concentrations of H_2 and O_2. Figure 8 displays the parietal field of the reactivity, which allows to put into evidence the regions that are prone to ignition. Downstream of the injection ($10.0 < x/D < 150.0$), the most reactive regions[4] are located on both sides of the hydrogen jet wake, as it is confirmed by the isocontour $0.95\,\langle\lambda\rangle_{\max}$, which is located in the vicinity of the abscissa $x/D = 60.0$. It is however noteworthy that, upstream of the injection, the reactivity values are even larger, see the top of Fig. 8. In this regard, according to the work of Gamba and Mungal [101] and Vincent-Randonnier *et al.* [91], it seems that this zone, which is associated to high levels of segregation between fuel and oxidizer, does not allow for ignition and combustion stabilization. This emphasizes the relevance of any modelling proposal, such as the one considered in reference [71], that considers the influence of a Damköhler

[4] In this region, the maximum value of the reactivity is $\lambda_{\max} = 434,500\ \mathrm{s}^{-1}$.

number based on the residence time τ_{res}, *i.e.*, $\text{Da} = \tau_{\text{res}}/\tau_{\text{igni}}$, the transport equation of which has been recently derived [105].

4. Analysis of the high-speed turbulent combustion regimes

All the results reported in this section have been obtained from the analysis and post-processing of the reactive flowfield computation.

The present geometry corresponds to a separated injection of the fuel in the oxidizer stream but the molecular mixing processes that take place between them — before combustion stabilization occurs — lead to a partially premixed mixture. The analysis of the reaction zone will therefore benefit from the evaluation of the degree of premixing between fuel and oxidizer. Thus, with the objective of distinguishing between the two limits of non-premixed ($\zeta_p = 0.0$) and premixed combustion ($\zeta_p = 1.0$), a premixedness index ζ_p or flame index (FI) [106, 107] will be considered. It is presently evaluated from $\zeta_p = (1.0 + \boldsymbol{n}_{\text{F}} \cdot \boldsymbol{n}_{\text{O}})/2.0$, where the quantities $\boldsymbol{n}_{\text{F}}$ and $\boldsymbol{n}_{\text{O}}$ denote unit vectors normal to iso-contours of the fuel and oxidizer mass fractions, respectively. It will be used to delineate locations that can be identified as premixed regions. As shown in Fig. 9, both premixed and non-premixed contributions are relevant to the present configuration. An illustration of this distribution is provided in Fig. 10, which depicts the instantaneous flame structure obtained at $t^* = 170.0$. This figure displays both OH and premixedness index distributions on the stoichiometric iso-surface. It shows that chemical reactions indeed proceed in a partially premixed combustion mode featuring premixed combustion in the vicinity of the stabilization zone. One may also notice that the water vapor present in the vitiated airstream leads to a slight production of OH radicals at the bow shock location, which is clearly visible on the parietal field of OH concentration displayed at the top of Fig. 10.

Since chemical reactions take place rather far downstream of the hydrogen injection port, after molecular mixing proceeds between hydrogen and high temperature vitiated air, combustion develops not only in partially premixed mixtures but also in high temperature conditions, *i.e.*, above the crossover [108]. Therefore, it is essential to attempt to discriminate between two possible physical mechanisms: flame propagation and ignition processes, which may be both involved in combustion stabilization. Thus, a simple preliminary study has been conducted on the basis of *(i)* one-dimensional premixed flame and *(ii)* homogeneous reactor computations so as to distinguish between the two phenomena (flame propagation and ignition). These computations are performed considering various mixtures of fresh reactants at

a temperature given by the expression introduced above, *i.e.*, $T_{\text{mix}} = T_u(\xi)$, and since pressure variations were found to remain negligible in the region where chemical reactions proceeds, these computations are performed in isobaric conditions at $p_0 = 56$ kPa, whatever the value of the mixture fraction.

Figure 11 displays the evolution of the ignition delay as a function of the mixture fraction ξ (top of the figure) and equivalence ratio Φ (bottom of the figure). The evolution of the unburnt mixture temperature $T_u(\xi)$ is also depicted. It is quite remarkable that the reactivity λ provides an excellent estimate of the ignition delay without requiring any numerical integration of the chemical system. Moreover, this set of curves puts into evidence the strong non-linearity of the ignition delay variation with the mixture fraction ξ. This characteristic time is very long for lean mixtures, decreases as the mixture fraction value is increased, until it reaches a local minimum, *i.e.*, the most reactive condition [109], and then sharply increases for richer mixtures. The most reactive state (*i.e.*, ξ_{mr}), which is estimated from the minimum ignition delay time, does not correspond to stoichiometry (*i.e.*, ξ_{st} or $\Phi = 1.0$) but to a mixture fraction value that is approximately equal to 0.0065 (*i.e.*, $\Phi_{\text{mr}} = 0.207$). This is a direct consequence of the significant temperature difference between the (cold) fuel stream and the (hot) oxidizer stream. It is also remarkable that the self-ignition delay displays a sharp increase for rich conditions in such a manner that spontaneous ignition regimes are less likely for these rich mixtures. More precisely, the corresponding ignition regimes require more time to develop, which may favor flame propagation mechanism. We will see below that flame propagation time scales indeed remain significantly smaller than ignition delays for such rich mixtures. However, as long as lean conditions are considered, only the ignition processes are expected to occur.

Figure 12 reports the evolution of the planar unstrained premixed laminar flame speed S_L^0 and its thermal thickness δ_L^0 as a function of the mixture fraction. This figure complements Fig. 11 in terms of the mixture fraction variation domain $\xi \in [0.0, 1.0]$. Indeed, in Fig. 12, only the domain $\xi \in [0.04, 0.30]$ is represented since, below the minimum bound, only ignition processes become relevant. Indeed, beyond this limit, the values of the laminar flame speed and thickness display unphysical variations from one computation to another and the corresponding results strongly depend on numerical simulation parameters (computational domain length, number of points, time-step, etc.) Finally, on the other side, beyond the maximum limit, the laminar flame speed tends towards zero: the high flammability limit is reached. The flame propagation velocity is indeed significantly decreased as the mixture fraction is increased beyond 0.3. It should reach

a maximum (together with a minimum flame thickness) in the vicinity of stoichiometry or most reactive condition but the ignition mechanism is the leading and controlling process for these mixtures.

4.1. Turbulent combustion regimes in the Barrère-Borghi coordinates

In order to determine the variability of the premixed combustion regime in the present JISCF configuration, the data are first displayed as a scatter-plot in a diagram that is commonly referred to as the Borghi diagram. The corresponding set of coordinates, introduced in reference [73, 111–113], corresponds to *(i)* a dimensionless velocity ratio u'/S_L^0, with u' (or $u_{\rm rms}$) the root-mean-square (RMS) of velocity fluctuation normalized by the laminar flame propagation velocity S_L^0, and *(ii)* a dimensionless length scale ratio L_t/δ_L^0, *i.e.*, the turbulent integral scale L_t normalized by the laminar flame thickness δ_L^0. In the following, the characteristic velocity fluctuation u' os evaluated from the resolved turbulent kinetic energy k, *i.e.*, $u' = \sqrt{2\,k/3}$, and the integral length scale L_t is estimated from $L_t = u'^3/\varepsilon$ with ε the resolved dissipation rate.

To proceed with the construction of this diagram the characteristics of the laminar premixed flame, *i.e.*, S_L^0 and δ_L^0, are evaluated only in a restricted part of the computational domain which is associated to *(i)* a probability that the flame index ζ_p exceeds a threshold value[5] larger than ten percent (this quantity is hereafter denoted by $P_{\rm PCZ}$) and *(ii)* mixture fraction values ξ within the range [0.04, 0.3] which, according to Fig. 12, correspond to reactive mixtures within which a premixed flame may propagate. This is in contrast with most of previous analyses of turbulent combustion regimes [114–117] where the corresponding quantities, *i.e.*, S_L^0 and δ_L^0, were generally evaluated from one single condition in terms of equivalence ratio, operating pressure, and fresh reactants temperature.

The corresponding set of data is presented in Fig. 13. This figure shows that, at $z/D = 0.0$ (see Fig. 13(c)), premixed combustion regimes are highly variable from one location to another. Possible combustion regimes include quasi-laminar premixed flame, thick flames, thickened flames, and thickened-wrinkled flames. In the near-wall region ($y/D = 0.0$ and $y/D = 0.25$), the laminar flame regimes predominate, see Figs. 13(a) and 13(b). Overall, the most significant heat release rate (HRR) values are associated to a Damköhler number smaller than unity. The turbulence time scales are rather small compared to the chemical time scales that are deduced from the flame propa-

[5] The threshold value ζ_p^{lim} is set to 0.7.

gation characteristics: chemistry can be considered as slow. The most probable regimes are associated to values of the Karlovitz number $\mathrm{Ka} = \left(\delta_L^0/\eta\right)^2$ that are significantly larger than unity: the thin flame assumption does not hold. Farther from the wall and injection port, the present set of results shows that values of the Damköhler number Da can exceed unity and that wrinkled flame regimes can be reached.

The scatterplot issued from the data collected in the medium plane ($z/D = 0.0$), see Fig. 13(c), is quite similar to the one issued from the Reynolds-averaged Navier-Stokes numerical simulation of the HIFiRE Direct Connect Rig geometry conducted by Quinlan *et al.* [77]. Compared to our results, the sole remarkable difference is a slight shift of the distribution upwards on the right ; the distribution reported by Quinlan *et al.* [77] features a *tongue* in the neighborhood of $(L_t/\delta_L^0, u'/S_L^0) = (0.10, 10.0)$ following the isoline $\mathrm{Ka} = 100.0$ up to values of L_t/δ_L^0 approximately equal to one hundred. As shown in the scatterplot gathered at $z/D = 0.0$ (see Fig. 13), the distribution issued from our own computational data features a quite similar *tongue* but it is following the isoline $\mathrm{Ka} = 20.0$ (instead of $\mathrm{Ka} = 100.0$). This dissemblance may be readily explained by the differences in terms of geometry (including cavities, multiple injections, etc.) and operating point (pressure, temperature, equivalence ratio, and fuel).

Together with those previously obtained by Quinlan *et al.* [77], the present results show that the wall boundary conditions significantly influence the dispersion of the observed premixed turbulent combustion regimes. In particular, it seems that the Karlovitz number value remains almost constant in the direct vicinity of the wall and the corresponding value is expected to depend on the studied configuration.

4.2. Turbulent combustion regimes in the (Re_t,Da)-coordinates

To complete the above combustion regime analysis, which was focused on the premixed flame propagation mode, we consider now turbulent combustion diagrams based on the couple $(\mathrm{Re}_t, \mathrm{Da})$. The corresponding representation is often referred to as the Williams coordinates. The most probable domains associated with supersonic combustion regimes, delineating the operating range of scramjets, were previously analyzed in such diagrams by Balakrishnan and Williams [75] and Ingenito and Bruno [76]. The corresponding domains will be depicted with red, blue, and green dotted lines in the figures discussed below. The definition of these domains are based on the consideration of a flight Mach number value that lies between 1.0 and 4.0 in reference [75] while the values $7.0-9.0$ were considered in reference [76]. Temperature values within the range $300.0 - 1200.0$ K were retained in the anal-

ysis conducted by Balakrishnan and Williams [75], while a value of 1000.0 K was used in reference [76]. Balakrishnan and Williams considered very high levels of turbulence intensity in the combustion chamber (*i.e.*, up to 50.0 %) while values $0.5-10.0$ % were retained as relevant ones in reference [76]. For the integral scale L_t, Balakrishnan and Williams [75] considered the dimensions of the combustion chamber as a reference length scale and chemical scales were determined from strained diffusion flamelets. The most probable supersonic combustion regimes, *i.e.*, those that are likely to be encountered in scramjets, were thus delineated [75]. However, as stated by the authors, this does not take into account the possible influence of the heat release on the turbulent kinetic energy, an influence that would lead to its decrease through the temperature-induced increase in viscosity. Lastly, there were still some uncertainties about the possible effects of ignition, which could alter the low limit of the possible supersonic combustion range. Ingenito and Bruno [76] defined this possible domain of supersonic combustion regimes through the analysis of single-step chemistry LES computations of the SCHOLAR benchmark. To conclude this brief introduction, it should be acknowledged that there are some uncertainties that remain regarding the possible impact of the fuel injection strategy and combustion chamber geometry, which has a significant influence on the mixing processes development and resulting Damköhler number values. As shown by Berglund *et al.* [118, 119], it is possible to evolve from flamelet regimes to distributed combustion regimes by switching from one configuration to another. The conclusions of such combustion regime studies are also expected to depend on the specification of boundary conditions.

From a general viewpoint, the Damköhler number, which is used as the ordinate in the combustion diagram, is estimated from $\mathrm{Da} = \tau_t/\tau_c$ with $\tau_t = L_t/u'$, the large eddy turnover time and τ_c, a chemical time scale. In the following, we will consider three distinct possibilities for estimating the value of this chemical time scale, which will be based *(i)* on the water vapor production rate, *(ii)* on the laminar premixed flame transit time δ_L^0/S_L^0, and *(iii)* on the ignition delay as deduced from the reactivity λ [103, 104]. These various time scales make possible the definition of Damköhler number based on *(i)* water vapor production rate ($\mathrm{Da}_{\mathrm{H_2O}}$), *(ii)* flame propagation mechanisms (Da_L), and *(iii)* ignition processes (Da_i), respectively. The turbulent Reynolds number, which appears as the abscissa of the combustion diagram, will be evaluated from $\mathrm{Re}_t = L_t u'/\langle\nu\rangle = k^2/\langle\nu\rangle\,\varepsilon$.

In a first step of this analysis, we consider a diagram based on the same definition as the one previously retained by Ingenito and Bruno [76]: we use the inverse of the production rate of water vapor as the relevant chemical

time scale. Figure 14 presents the corresponding $(\mathrm{Re}_t, \mathrm{Da}_{\mathrm{H_2O}})$ combustion diagram. It shows that the obtained supersonic combustion regimes lie below the zone delineated by Ingenito and Bruno [76]. This result is fully consistent with the study of Cock [120] who scrutinized the effects (on Damköhler number estimates) of a multi-step finite-rate chemical kinetics description compared to a single-step chemistry. The large gap, of about two decades, that is observed between the present set of results and those documented in reference [76], is thus ascribed to the use of a finite-rate multi-step chemistry.

Moreover, the present set of results lies in the vicinity of the low boundary (*i.e.*, minimum bounds in Re_t and $\mathrm{Da}_{\mathrm{H_2O}}$) of the possible domain defined by Balakrishnan and Williams [75], which is depicted in blue color in Fig. 14. At this level, it is noteworthy that, as emphasized by Balakrishnan and Williams, the main effect of heat release is to reduce the turbulent kinetic energy, an effect that has not been considered in the delineation of the corresponding domain in reference [75]. The work of Cock [120] and the more recent analysis of Fureby [121] also documented the way the heat release may alter the turbulence intensity in high-speed flow conditions. The results of reference [121] feature very large compressibility effects, with turbulent Mach number values of the order of 1.5 while the turbulent Reynolds number values lie between 10^2 and 10^4. In the present conditions, a decrease in the turbulence intensity from ten to five percent is observed across the reactive zone. This is in good agreement with the observations made by Ingenito and Bruno [76] but it should be however emphasized that larger turbulence intensity can be expected in confined conditions.

In a second step of the analysis, a Damköhler number based on the flame propagation mechanism is considered. The resulting $(\mathrm{Re}_t, \mathrm{Da}_L)$ diagram is reported in Fig. 15. The regions that are not representative of a flame propagation mechanism are excluded from the analysis by using the same conditioning (based on the premixedness probability and mixture fraction limits) as the one introduced in the previous subsection. Figure 15 shows that, in comparison to the data presented above, the scatterplot has been translated upwards by about one decade to reach the broken flamelets regime, above the slow chemistry limit $\mathrm{Da}_L = 1.0$ limit. The tapered shape of the scatterplot follows the isoline $\mathrm{Ka}_L = 100.0$. It is noteworthy that this differs from the regimes delineated above in the Barrère-Borghi coordinates. This is just a consequence of the unity flame Reynolds number assumption, *i.e.*, $S_L^0 \delta_L^0 / \nu = 1.0$, which is not perfectly verified; the boundaries that are delineated in the Borghi diagram are indeed based on this assumption, which is used to relate the Damköhler, Karlovitz, and Reynolds numbers: $\mathrm{Re}_t = \mathrm{Da}_L^2 \mathrm{Ka}_L^2$. The scatterplot reaches the regions that were previously

delineated for supersonic combustion regimes in the studies of Balakrishnan and Williams [75] and Ingenito and Bruno [76]. Most of the heat release rate takes place in the PSR regime as already shown above in the premixed turbulent combustion diagram (see Fig. 13).

The diagram displayed in Fig. 15(a) shows that the points where the probability to lie within a premixed combustion zone is the most important are gathered around the isoline $\mathrm{Da}_L = 1.0$ and lie within the broken flamelets regime, which can be associated to thickened-wrinkled flame regime in the Barrère-Borghi coordinates. This region is also characterized by supersonic flow conditions (*i.e.*, Ma > 1.0). In this respect, the combustion diagram reported in Fig. 15(c) also indicates that the sonic line follows closely the low limit of the supersonic combustion regimes delineated by Ingenito and Bruno [76]. As pointed out by Balakrishnan and Williams [75], this diagram does incorporate neither the compressibility nor the high-Mach number effects, which can be important in high-speed flow conditions. Thus, the turbulent Mach number, which provides a measure of compressibility effects on turbulence, has been also considered. Its value is significant (between 0.2-0.3) in regions where the heat release rate is highest, *i.e.*, in the vicinity of the wall ($y/D < 1.0$), then it decreases in the regions that are associated to the broken flamelet regime. At this level, it is noteworthy that Fureby [121] has conducted a similar analysis on the HyShot II configuration. In this study important compressibility effects were put into evidence, with turbulent Mach number values that can be locally as high as 1.5. The corresponding regions are under the influence by the counter-rotating vortices pair (CVP), shock reflection, and shock-induced ignition. Indeed, in the simulated geometry, the shock train certainly allows for the persistence of a high level of velocity fluctuations at each reflected shock wave crossing. Finally, the last two diagrams reported in Figs. 15(e) and 15(f) display the scatterplots colored by the normalized coordinates and thus allow to identify the flow regions in which the various turbulent combustion regimes develop. In the near wall region and in the vicinity of the injection port, the combustion regime is mostly that of a PSR, while farther from the wall and hydrogen injection, the broken flamelets regime is the most probable.

The combustion regime analysis is ended by considering a Damköhler number definition that is based on the ignition delay. The resulting turbulent combustion diagrams are displayed in Fig. 16. Since the corresponding definition does not account for any flame structure (the retained time scale is indeed deduced from homogeneous reactor computations), the regimes relevant to such flame structures are no longer referred to in these diagrams. Thus, only three sub-domains are considered: the laminar regime, the PSR

or slow chemistry regime, and the fast chemistry regime. Compared to the previous set of diagrams, the scatterplots displayed in Fig. 16 exhibit some thickening since the number of points under consideration has been significantly increased: the sole conditioning that is applied corresponds to a simple thresholding of the heat release rate (one tenth percent of its maximum value). First, it is noteworthy that the scatterplot has been translated upwards by about one decade in comparison with the previous results obtained with a Damköhler number definition based on laminar premixed flamelets. The distribution features larger values of the Damköhler number. This confirms that, even if combustion takes place in the direct vicinity of the wall, the principal mechanism for combustion stabilization is related to ignition rather than flame propagation. One can also notice that the elongated part of the distribution now varies between $\mathrm{Ka}_i = 1.0$ and $\mathrm{Ka}_i = 20.0$. Moreover, it is quite remarkable that, with the present definition of the Damköhler number, the scatterplots is in satisfactory agreement with supersonic combustion regime regions previously delineated by Ingenito and Bruno [76] and by Balakrishnan and Williams [75]. In contrast to the previous set of data relevant to premixed flame propagation (see Fig. 15), the present set of results — which does account for the contribution of ignition processes — shows that the most important HRR values are associated to fast chemistry regimes featuring $1.0 < \mathrm{Da}_i < 100.0$. Figure 16(a) also confirms that the regions associated to significant HRR values correspond to moderate SDR (with the SDR evaluated from its resolved contribution), *i.e.*, conditions which are favourable to the development of ignition processes [109].

The inspection of the Mach number shows that the fast chemistry regimes ($1.0 < \mathrm{Da}_i < 100.0$) are relevant to supersonic flow conditions ($\mathrm{Ma} > 1.2$). The turbulent Mach number values indicate that the compressibility effects are important in the near wall region $y/D < 1.0$, *i.e.*, in regions featuring significant heat release rates.

5. Conclusions and prospects

High-speed turbulent combustion regimes are analyzed in standard combustion diagrams based on *(i)* either the Barrère-Borghi coordinates or *(ii)* in the $(\mathrm{Re}_t, \mathrm{Da})$-plane, which is often referred to as the Williams coordinates. Since they rely on dimensional reasoning and scaling principles, the various boundaries that delineate the corresponding regimes have been early and continuously questioned over the years [122, 123]. In this respect, it seems worth recalling that such diagrams were introduced almost fifty years ago so as to provide a rather qualitative view of the possible evolution of turbulent

combustion interactions as the characteristic length and time scales of the turbulent flowfield and/or chemistry are varied. Despite the intrinsic limitations of this overly simplified picture of turbulence-chemistry interactions, such heuristic diagrams do provide a quite valuable point of view and it is quite remarkable that, still today, they are retained as a first useful step to characterize turbulent combustion setups and they concentrate a significant amount of research works. For instance, some insights onto the limit of flamelet broadening have been recently gained from experimental and computational studies of premixed flames subject to intense turbulence [124, 125]. The interaction of high-speed turbulence with premixed flames has been also investigated by Poludnenko and Oran [126, 127] and several DNS studies have been focused on combustion regimes featuring large values of the Karlovitz number [128–131]. For such conditions, it is quite remarkable that, in contrast to the standard picture of thickened flame regimes, some local thicknesses (*e.g.*, norms of the species mass fraction gradient of intermediate species like carbon monoxide) do exhibit thinning rather than broadening effects. Moreover, in contrast to the picture of a large and nearly homogenous reaction zone, high-fidelity imaging of the flame structure and topology has shown that extreme turbulence may lead to the formation of distributed reaction pockets (or blobs) that are connected by thin flamelets [132, 133]. As emphasized in reference [134], such a topology displays some similarities with the Shchetinkov's picture of micro-volume combustion regime and his early analysis of combustion processes in a scramjet [135, 136].

In comparison to these studies, which are mostly concerned with fully-premixed combustion in low Mach number flows, the present analysis is conducted in conditions relevant to scramjet operations with a separated injection of the fuel in a supersonic vitiated airstream. The consideration of such conditions rises some specific issues. For instance, additional effects related to high Mach number values and compressibility may be expected, which require in principle the extension of combustion diagrams to additional dimensions. However, the Damköhler and Reynolds numbers, *i.e.*, the ratio of flow to chemical time (or lenght) scales are deemed the two most significant parameters. Thus, the difficulty of multi-dimensional diagrams (with a number of dimensions larger than two) is presently circumvented by considering combustion regime scatterplots in the standard sets of coordinates but colored by other relevant quantities: Ma, Ma_t, SDR, etc. In addition to this, various Damköhler number definitions have been considered based on either premixed flame propagation or ignition characteristics so as to evaluate relevant time and length scales. Whatever the definition, this analysis puts into evidence turbulent combustion regimes featuring significant finite-rate

chemical kinetics effects. The obtained results show the wide variety of combustion regimes involved in such high-speed flow conditions. Most of them have however something in common : they lie above the Klimov-Williams limit (Ka > 1.0). This analysis also reveals that, for the conditions that are studied, the largest values of the HRR are obtained in the vicinity of the wall ($y/D < 1.0$). At the corresponding locations, the reactive mixture features a significant level of premixing. These conditions are also associated to the largest values of the turbulent Mach number (Ma_t ranges between 0.12 and 0.35) and correspond to almost sonic conditions. This emphasizes the relevance of future work devoted to the wall physics (heat transfer, wall roughness, etc.). The influence of wall boundary conditions indeed remains to be more largely addressed since it can significantly affect the near wall flow dynamics of recirculation regions interacting with redeveloping boundary layers. From a more general point of view, the effects of the confinement (*e.g.*, shock reflection and interaction, resulting SWBLI, etc.) also deserve to be analyzed.

To conclude, the physics of high-speed turbulent combustion regimes is not the sole concern in the application of supersonic combustion for possible future hypersonic flight. Combustion in scramjet rise other challenging issues for better optimizing the ratio of residence time over chemical times while ensuring stabilization of combustion. Fundamental physical aspects related to compressibility effects competing with significant heat release, affecting in a different way both large and small turbulent scales need to be addressed. In particular the control of combustion stabilization mechanisms in high-speed reacting flows first requires a deeper understanding of the numerous sources of unsteadiness associated to shock wave/mixing layers or shock wave/boundary layers interactions (SWBLI). A competition between so-called compressibility effects, reducing the spreading rate of free shear layers, heat release and/or, on the contrary, enhancement of large-scale instability modes in injection jet for particular physical or geometrical conditions can tremendously affect the subsequent mixing of reactants. Combined with experiments, the use of high-fidelity tools should be intensified to get further insights into these complex interactions and possibly improve the efficiency of low-order models for optimization. Answering the above issues may require some modelling efforts. For instance, most of the sub-grid scale turbulence and multi-regime combustion models have never been assessed for such extreme conditions. Finally, the relevance of existing chemical kinetics descriptions should also be questioned for these rapidly-variable temperature and pressure conditions.

The above lines have been written to pay tribute to K.N.C. Bray's contribution in the field of turbulent combustion modelling. The focus has been placed on combustion in supersonic flows, a topic on which his input in the seventies and nineties was also significant. Before concluding this manuscript, it seems worth emphasizing that Professor Bray is not only recognized to be one amongst the most prominent and renowned scientists in the international combustion community, he is also one amongst its most appreciated figures: an eminent scientist who is known as a gentleman.

6. Acknowledgments

This work has benefited from discussions on supersonic flows and high-speed combustion shared with colleagues and former PhD students and especially with R. Borghi, R. Buttay, M. Champion, P. Comte, L.F. Figueira da Silva, M. Ferrier, C. Fureby, T. Gatski, A. Hadjadj, J.F. Izard, P.J. Martinez-Ferrer, Y. Moule, V.A. Sabelnikov, D. Scherrer, and A. Vincent-Randonnier.

This research on supersonic combustion has been partly funded by Airbus Group (MBDA) within the framework of the International Chair *Propulsion and Environment*. It was granted access to important HPC resources of IDRIS under the allocations i20162b7251 made by GENCI (*Grand Equipement National de Calcul Intensif*).

References

[1] K. N. C. Bray, P. A. Libby, Interaction effects in turbulent premixed flames, Phys. Fluids 19 (1976) 1687–1701.

[2] K. N. C. Bray, J. B. Moss, A unified statistical model of the premixed turbulent flame, Acta Astronaut. 4 (1977) 291–319.

[3] K. N. C. Bray, J. B. Moss, A closure model for the turbulent premixed flame with sequential chemistry, Combust. Flame 30 (1977) 125–131.

[4] K. N. C. Bray, The interaction between turbulence and combustion, Symp. (Int.) Combust. 17 (1979) 223–233.

[5] P. A. Libby, K. N. C. Bray, Implications of the laminar flamelet model in premixed turbulent combustion, Combust. Flame 39 (1980) 33–41.

[6] K. N. C. Bray, Turbulent flows with premixed reactants, in: P. A. Libby, F. A. Williams (Eds.), Turbulent Reacting Flows, Topics in Applied Physics, vol. 44, Springer, Berlin, Heidelberg, 1980, pp. 115–183.

[7] K. N. C. Bray, P. A. Libby, G. J. Masuya, J. B. Moss, Turbulence production in premixed turbulent flames, Combust. Sci. Technol. 25 (1981) 127–140.

[8] P. A. Libby, K. N. C. Bray, Counter gradient diffusion in premixed turbulent flames, AIAA J. 19 (1981) 205–213.

[9] K. N. C. Bray, Studies of the turbulent burning velocity, Proc. R. Soc. Lond. A 431 (1990) 315–335.

[10] K. N. C. Bray, R. S. Cant, Some applications of Kolmogorov's turbulence research in the field of combustion, Proc. R. Soc. Lond. A 434 (1991) 217–240.

[11] K. N. C. Bray, N. Peters, Laminar flamelets in turbulent flames, in: P. A. Libby, F. A. Williams (Eds.), Turbulent Reacting Flows, Academic Press, San Diego, 1994, pp. 63–113.

[12] K. N. C. Bray, Turbulent transport in flames, Proc. R. Soc. Lond. A 451 (1995) 231–256.

[13] K. N. C. Bray, The challenge of turbulent combustion, Symp. (Int.) Combust. 26 (1996) 1–26.

[14] D. Veynante, A. Trouvé, K. N. C. Bray, T. Mantel, Gradient and counter-gradient scalar transport in turbulent premixed flames, J. Fluid Mech. 332 (1997) 263–293.

[15] P. Domingo, K. N. C. Bray, Laminar flamelet expressions for pressure fluctuation terms in second moment models of premixed turbulent combustion, Combust. Flame 121 (2000) 555–574.

[16] R. W. Bilger, S. B. Pope, K. N. C. Bray, J. F. Driscoll, Paradigms in turbulent combustion research, Proc. Combust. Inst. 30 (2005) 21–42.

[17] N. Swaminathan, K. N. C. Bray, Effect of dilatation on scalar dissipation in turbulent premixed flames, Combust. Flame 143 (2005) 569–565.

[18] K. N. C. Bray, M. Champion, P. A. Libby, Premixed flames in stagnating turbulence: Part I. The general formulation for counterflowing streams and gradient models for turbulent transport, Combust. Flame 84 (1991) 391–410.

[19] K. N. C. Bray, M. Champion, P. A. Libby, Premixed flames in stagnating turbulence: Part II. The mean velocities and pressure and the Damköhler number, Combust. Flame 112 (1998) 635–653.

[20] K. N. C. Bray, M. Champion, P. A. Libby, Premixed flames in stagnating turbulence: Part III. The $k - \epsilon$ theory for reactants impinging on a wall, Combust. Flame 91 (1992) 165–186.

[21] K. N. C. Bray, M. Champion, P. A. Libby, Premixed flames in stagnating turbulence: Part IV. A new theory for the Reynolds stresses and Reynolds fluxes applied to impinging flows, Combust. Flame 120 (2000) 1–18.

[22] K. N. C. Bray, M. Champion, P. A. Libby, Premixed flames in stagnating turbulence: Part V. Evaluation of models for the chemical source term, Combust. Flame 127 (2001) 2023–2040.

[23] K. N. C. Bray, M. Champion, P. A. Libby, Premixed flames in stagnating turbulence: Part VI. Predicting the mean density and the permitted rates of strain for impinging reactant streams, Combust. Flame 156 (2009) 310–321.

[24] P. Bailly, M. Champion, D. Garreton, Counter-gradient diffusion in a confined turbulent premixed flame, Phys. Fluids 9 (1997) 766–775.

[25] S. Nishiki, T. Hasegawa, R. Borghi, R. Himeno, Modeling of flame-generated turbulence based on direct numerical simulation databases, Proc. Combust. Inst. 29 (2002) 2017–2022.

[26] Y. H. Im, K. Y. Huh, S. Nishiki, T. Hasegawa, Zone conditional assessment of flame-generated turbulence with DNS database of a turbulent premixed flame, Combust. Flame 137 (2004) 478–488.

[27] N. Chakraborty, N. Swaminathan, Influence of the Damköhler number on turbulence-scalar interaction in premixed flames.Part I: Physical insight, Phys. Fluids 19 (2007) 045103.1–045103.10.

[28] A. Mura, K. Tsuboi, T. Hasegawa, Modelling of the correlation between velocity and reactive scalar gradients in turbulent premixed flames based on DNS data, Combust. Theor. Model. 12 (2008) 671–698.

[29] V. Robin, M. Champion, A. Mura, A second-order model for turbulent reactive flows with variable equivalence ratio, Combust. Sci. Technol. 180 (2008) 1709–1734.

[30] A. N. Lipatnikov, Conditionally averaged balance equations for modeling premixed turbulent combustion in flamelet regime, Combust. Flame 152 (2008) 529–547.

[31] A. Mura, M. Champion, Relevance of the Bray number in the small-scale modeling of turbulent premixed flames, Combust. Flame 156 (2009) 729–733.

[32] P. E. Hamlington, A. Y. Poludnenko, E. S. Oran, Interactions between turbulence and flames in premixed reacting flows, Phys. Fluids 23 (2011) 125111.

[33] V. Robin, A. Mura, M. Champion, Direct and indirect thermal expansion effects in turbulent premixed flames, J. Fluid Mech. 689 (2011) 149–182.

[34] R. Yu, X. S. Bai, A. N. Lipatnikov, A direct numerical simulation study of interface propagation in homogeneous turbulence, J. Fluid Mech. 772 (2015) 127–164.

[35] K. Kha, V. Robin, A. Mura, M. Champion, Implications of laminar flame finite thickness on the structure of turbulent premixed flames, J. Fluid Mech. 787 (2016) 116.

[36] V. A. Sabelnikov, A. N. Lipatnikov, Recent advances in understanding of thermal expansion effects in premixed turbulent flames, Annu. Rev. Fluid Mech. 49 (2017) 91–117.

[37] L. Tian, R. P. Lindstedt, The impact of dilatation, scrambling, and pressure transport in turbulent premixed flames, Combust. Theor. Model. 21 (2017) 1114–1147.

[38] S. Zhao, A. Er-raiy, Z. Bouali, A. Mura, Dynamics and kinematics of the reactive scalar gradient in weakly turbulent premixed flames, Combust. Flame 198 (2018) 436–454.

[39] J. F. MacArt, T. Grenga, M. E. Mueller, Effects of combustion heat release on velocity and scalar statistics in turbulent premixed jet flames at low and high Karlovitz numbers, Combust. Flame 191 (2018) 468–485.

[40] V. A. Sabelnikov, A. N. Lipatnikov, S. Nishiki, T. Hasegawa, Investigation of the influence of combustion-induced thermal expansion on

two-point turbulence statistics using conditioned structure functions, J. Fluid Mech. 867 (2019) 45–76.

[41] A. Mura, S. Zhao, Turbulence topology evolution in weakly turbulent premixed flames, Phys. Fluids (2021) 33 (2021) 035110.

[42] T. Mantel, R. Borghi, A new model of premixed wrinkled flame based on a scalar dissipation equation, Combust. Flame 96 (1994) 443–457.

[43] A. Mura, R. Borghi, Towards an extended scalar dissipation equation for turbulent premixed combustion, Combust. Flame 133 (2003) 193–196.

[44] A. Mura, F. Galzin, R. Borghi, A unified PDF-flamelet model for turbulent premixed combustion, Combust. Sci. Technol. 175 (2003) 1573–1609.

[45] V. Robin, A. Mura, M. Champion, P. Plion, A multi-dirac presumed PDF model for turbulent reactive flows with variable equivalence ratio, Combust. Sci. Technol. 178 (2006) 1843–1870.

[46] A. Mura, V. Robin, M. Champion, Modeling of scalar dissipation in partially premixed turbulent flames, Combust. Flame (2007) 217–224.

[47] H. Kolla, N. Swaminathan, Strained flamelets for turbulent premixed flames. I: Formulation and planar flame results, Combust. Flame 157 (2010) 943–954.

[48] H. Kolla, N. Swaminathan, Strained flamelets for turbulent premixed flames. II: Laboratory flame results, Combust. Flame 157 (2010) 1274–1289.

[49] D. Butz, Y. Gao, A. Kempf, N. Chakraborty, Large eddy simulations of a turbulent premixed swirl flame using an algebraic scalar dissipation rate closure, Combust. Flame 162 (2015) 3180–3196.

[50] I. Langella, N. Swaminathan, R. W. Pitz, Application of unstrained flamelet SGS closure for multi-regime premixed combustion, Combust. Flame 173 (2016) 161–178.

[51] K. N. C. Bray, Atomic recombination in a hypersonic wind-tunnel nozzle, J. Fluid Mech. 6 (1959) 1–32.

[52] J. P. Appleton, K. N. C. Bray, The conservation equations for a non-equilibrium plasma, J. Fluid Mech. 20 (1964) 659–672.

[53] K. N. C. Bray, Vibrational relaxation of anharmonic oscillator molecules: Relaxation under isothermal conditions, J. Phys. B. Atom. Molec. Phys. 1 (1968) 705–717.

[54] M. W. Slack, K. N. C. Bray, R. A. East, N. H. Pratt, Steady expansion of shock-heated gases for recombination studies, Phys. Fluids 12 (1969) 113–117.

[55] K. N. C. Bray, Vibrational relaxation of anharmonic oscillator molecules. II. non- isothermal conditions, J. Phys. B. Atom. Molec. Phys. 3 (1970) 1515–1538.

[56] C. W. von Rosenberg, N. H. Pratt, K. N. C. Bray, Absolute H_2O ν_2-band intensity obtained from reacting $H_2 + O_2$ mixtures behind shock waves, J. Quant. Spectrosc. Radiat. Transf. 10 (1970) 1155–1169.

[57] C. W. von Rosenberg, K. N. C. Bray, N. H. Pratt, Shock tube vibrational relaxation measurements: N_2 relaxation by H_2O and the $CO - N_2$ V-V rate, J. Chem. Phys. 56 (1972) 3230–3237.

[58] E. Oran, Astrophysical combustion, Proc. Combust. Inst. 30 (2005) 1823–1840.

[59] A. Ferri, Mixing-controlled supersonic combustion, Annu. Rev. Fluid Mech. 5 (1973) 301–338.

[60] R. Buttay, L. Gomet, G. Lehnasch, A. Mura, Highly resolved numerical simulation of combustion downstream of a rocket engine igniter, Shock Waves 27 (2017) 655–674.

[61] W. H. Heiser, D. T. Pratt, Hypersonic airbreathing propulsion, AIAA Education Series, 1994.

[62] M. K. Smart, Scramjets, Tech. rep., RTO-EN-AVT-150-09 (2008).

[63] A. Ferri, P. A. Libby, V. Sakkay, Theoretical and experimental investigation of supersonic combustion, Tech. rep., Report ARL 62-467, Aeronautical Research Laboratory, Polytechnic Institute of Brooklyn, New York (1962).

[64] K. N. C. Bray, P. A. Libby, F. A. Williams, High-speed turbulent combustion, in: P. A. Libby, F. A. Williams (Eds.), Turbulent Reacting Flows, Academic Press, San Diego, 1994, pp. 609–638.

[65] P. A. Libby, Observations concerning supersonic combustion, in: M. Champion, B. Deshaies (Eds.), IUTAM Symposium on Combustion in Supersonic Flows. Fluid Mechanics and Its Applications, vol. 39, Springer, Dordrecht, 1997, pp. 1–11.

[66] L. L. Zheng, K. N. C. Bray, The application of new combustion and turbulence models to H_2-air non-premixed supersonic combustion, Combust. Flame 99 (1994) 440–448.

[67] K. H. Luo, K. N. C. Bray, Combustion-induced pressure effects in supersonic diffusion flames, Symp. (Int.) Combust. 27 (1998) 2165–2171.

[68] V. A. Sabelnikov, B. Deshaies, L. F. Figueira da Silva, Revisited flamelet model for nonpremixed combustion in supersonic turbulent flows, Combust. Flame 114 (1998) 577–584.

[69] J. F. Izard, G. Lehnasch, A. Mura, A Lagrangian model of combustion in high-speed flows: application to scramjet conditions, Combust. Sci. Technol. 181 (2009) 1372–1396.

[70] A. Mura, J. F. Izard, Numerical simulation of supersonic nonpremixed turbulent combustion in a scramjet combustor model, J. Propuls. Power 26 (2010) 858–868.

[71] L. Gomet, V. Robin, A. Mura, Influence of residence and scalar mixing time scales in non-premixed combustion in supersonic turbulent flows, Combust. Sci. Technol. 184 (2012) 1471–1501.

[72] P. J. Martínez Ferrer, G. Lehnasch, A. Mura, Compressibility and heat release effects in high-speed reactive mixing layers: structure of the stabilization zone and modeling issues relevant to turbulent combustion in supersonic flows, Combust. Flame 180 (2017) 304–320.

[73] R. Borghi, On the structure and morphology of turbulent premixed flames, in: C. Casci, C. Bruno (Eds.), Recent Advances in the Aerospace Sciences, Springer, Boston, MA, 1985, pp. 117–138.

[74] N. Peters, The turbulent burning velocity for large-scale and small-scale turbulence, J. Fluid Mech. 384 (1999) 107–132.

[75] G. Balakrishnan, F. A. Williams, Turbulent combustion regimes for hypersonic propulsion employing hydrogen-air diffusion flames, J. Propuls. Power 10 (1994) 434–437.

[76] A. Ingenito, C. Bruno, Physics and regimes of supersonic combustion, AIAA J. 48 (2010) 515–525.

[77] J. Quinlan, J. C. McDaniel, T. G. Drozda, G. Lacaze, J. C. Oefelein, A priori analysis of flamelet-based modeling for a dual-mode scramjet combustor, AIAA 2014-3743.

[78] R. Buttay, G. Lehnasch, A. Mura, Analysis of small-scale scalar mixing processes in highly under-expanded jets, Shock Waves 26 (2016) 93–212.

[79] P. J. Martínez Ferrer, G. Lehnasch, A. Mura, Compressibility and heat release effects in high-speed reactive mixing layers: growth rates and turbulence characteristics, Combust. Flame 180 (2017) 284–303.

[80] R. Boukharfane, Z. Bouali, A. Mura, Evolution of scalar and velocity dynamics in planar shock-turbulence interaction, Shock Waves 28 (2018) 1117–1141.

[81] A. Techer, Y. Moule, G. Lehnasch, A. Mura, Mixing of fuel jet in supersonic crossflow: Estimation of subgrid-scale scalar fluctuations, AIAA J. 56 (2018) 465–481.

[82] R. Buttay, G. Lehnasch, A. Mura, Turbulent mixing and molecular transport in highly under-expanded hydrogen jets, Int. J. Hydrog. Energy 43 (2018) 8488–8505.

[83] D. Martínez-Ruiz, C. Huete, P. J. Martínez Ferrer, D. Mira, Irregular self-similar configurations of shock-wave impingement on shear layers, J. Fluid Mech. 872 (2019) 889–927.

[84] R. Boukharfane, P. J. Martínez Ferrer, A. Mura, V. Giovangigli, On the role of bulk viscosity in compressible reactive shear layer developments, Eur. J. Mech. B Fluids 77 (2019) 32–47.

[85] J. Ciesko, M. F. P. J., R. Penacoba Veigas, X. Teruel, V. Beltran, HDOT – an approach towards productive programming of hybrid applications, J. Parallel. Distrib. Comput. 137 (2020) 104–118.

[86] F. H. E. Ribeiro, R. Boukharfane, A. Mura, Highly-resolved large-eddy simulations of combustion stabilization in a scramjet engine model with cavity flameholder, Comput. Fluids 197 (2020) 104344.

[87] D. Martínez-Ruiz, C. Huete, P. J. Martínez Ferrer, D. Mira, Specific heat effects in two-dimensional shock refractions, Shock Waves (2021) 31 (2021) 1–17.

[88] P. J. Martínez Ferrer, R. Buttay, G. Lehnasch, A. Mura, A detailed verification procedure for compressible reactive multicomponent Navier-Stokes solvers, Comput. Fluids 89 (2014) 88–110.

[89] R. Boukharfane, F. H. E. Ribeiro, Z. Bouali, A. Mura, A combined ghost-point-forcing / direct-forcing immersed boundary method (IBM) for compressible flow simulations, Comput. Fluids 162 (2018) 91–112.

[90] J. O. Hirschfelder, C. F. Curtiss, R. B. Bird, Molecular theory of gases and liquids, Wiley, 1954.

[91] A. Vincent-Randonnier, Y. Moule, M. Ferrier, Combustion of hydrogen in hot air flows within LAPCAT-II dual mode ramjet combustor at onera-LAERTE facility : experimental and numerical investigation, 19th AIAA International Space Planes and Hypersonic Systems and Technologies Conference (2014) AIAA Paper 2014–2932.

[92] A. Vincent-Randonnier, V. A. Sabelnikov, A. Ristori, N. Zettervall, C. Fureby, An experimental and computational study of hydrogen-air combustion in the LAPCAT II supersonic combustor, Proc. Combust. Inst. 37 (2019) 3703–3711.

[93] G. Pelletier, M. Ferrier, A. Vincent-Randonnier, V. A. Sabelnikov, A. Mura, Wall roughness effects on combustion development in confined supersonic flow, J. Propuls. Power 37 (2021) 151–166.

[94] S. B. Pope, Ten questions concerning the large-eddy simulation of turbulent flows, New J. Phys. 6 (2004) 35.

[95] I. B. Celik, Z. N. Cehreli, I. Yavuz, Index of resolution quality for large eddy simulations, J. Fluids Eng. 127 (5) (2005) 949–958.

[96] L. Bouheraoua, P. Domingo, G. Ribert, Large-eddy simulation of a supersonic lifted jet flame: Analysis of the turbulent flame base, Combust. Flame 179 (2017) 199–218.

[97] J. M. Vedovoto, A. Silveira Neto, L. F. Figueira da Silva, A. Mura, Influence of synthetic inlet turbulence on the prediction of low mach number flows, Comput. Fluids 106 (2015) 135–153.

[98] M. Gamba, V. E. Terrapon, A. Saghafian, M. G. Mungal, H. Pitsch, Assessment of the combustion characteristics of hydrogen transverse jets in supersonic crossflow, in: Center for Turbulence Research, Annual Research Briefs 2011, Stanford (CA, USA).

[99] A. Saghafian, V. E. Terrapon, H. Pitsch, An efficient flamelet-based combustion model for compressible flows, Combust. Flame 162 (3) (2015) 652–667.

[100] P. Boivin, A. L. Sánchez, F. A. Williams, Four-step and three-step systematically reduced chemistry for wide-range H_2-air combustion problems, Combust. Flame 160 (2013) 76–82.

[101] M. Gamba, M. G. Mungal, Ignition, flame structure and near-wall burning in transverse hydrogen jets in supersonic crossflow, J. Fluid Mech. 780 (2015) 226–273.

[102] M. Ó Conaire, H. J. Curran, J. M. Simmie, W. J. Pitz, C. K. Westbrook, A comprehensive modeling study of hydrogen oxidation, Int. J. Chem. Kinet. 36 (2004) 603–622.

[103] P. Boivin, C. Jiménez, A. L. Sánchez, F. A. Williams, An explicit reduced mechanism for H2-air combustion, Proc. Combust. Inst. 33 (2011) 517–523.

[104] P. Boivin, A. Dauptain, C. Jiménez, B. Cuenot, Simulation of a supersonic hydrogen-air autoignition-stabilized flame using reduced chemistry, Combust. Flame 159 (2012) 1779–1790.

[105] X. Wang, V. Robin, A. Mura, A normalised residence time transport equation for the numerical simulation of combustion with high-temperature air, Combust. Theor. Model. 23 (2019) 821–853.

[106] H. Yamashita, M. Shimada, T. Takeno, A numerical study on flame stability at the transition point of jet diffusion flames, Symp. (Int.) Combust. 26 (1996) 27–34.

[107] E. Illana, D. Mira, A. Mura, An extended flame index partitioning for partially premixed combustion, Combust. Theor. Model. 25 (2021) 121–157.

[108] A. L. Sánchez, F. A. Williams, Recent advances in understanding of flammability characteristics of hydrogen, Prog. Energy Combust. Sci. 41 (2014) 1–55.

[109] E. Mastorakos, T. A. Baritaud, T. J. Poinsot, Numerical simulations of autoignition in turbulent mixing flows, Combust. Flame 109 (1997) 198–223.

[110] C. J. Jachimowski, An analytical study of the hydrogen-air reaction mechanism with application to scramjet combustion, Tech. rep., NASA STI Technical Report (1988).

[111] M. Barrere, Modèles de combustion turbulente, Rev. Gen. Therm. 148 (1974) 295–308.

[112] M. Barrere, Quelques recherches sur la combustion de la dernière décennie, J. Chim. Phys. 81 (1984) 519–531.

[113] R. Borghi, Sur la structure des flammes turbulentes, J. Chim. Phys. 81 (1984) 361–370.

[114] H. Wang, K. Luo, S. Lu, J. Fan, Direct numerical simulation and analysis of a hydrogen/air swirling premixed flame in a micro combustor, Int. J. Hydrog. Energy 36 (2011) 13838–13849.

[115] Y. Minamoto, K. Aoki, M. Tanahashi, N. Swaminathan, DNS of swirling hydrogen-air premixed flames, Int. J. Hydrog. Energy 40 (2015) 13604–13620.

[116] P. Benard, Analyse et amélioration d'une chambre de combustion centimétrique par simulations aux grandes échelles, Ph.D. thesis, INSA de Rouen (2015).

[117] P. Benard, V. Moureau, G. Lartigue, Y. D'Angelo, Large-eddy simulation of a hydrogen enriched methane/air meso-scale combustor, Int. J. Hydrog. Energy 42 (2017) 2397–2410.

[118] M. Berglund, C. Fureby, LES of supersonic combustion in a scramjet engine model, Proc. Combust. Inst. 31 (2007) 2497–2504.

[119] M. Berglund, E. Fedina, C. Fureby, J. Tegnér, V. A. Sabelnikov, Finite-rate chemistry large-eddy simulation of self-ignition in supersonic combustion ramjet, AIAA J. 48 (2010) 540–550.

[120] P. A. T. Cocks, Large-eddy simulation of supersonic combustion with application to scramjet engines, Ph.D. thesis, University of Cambridge (2011).

[121] C. Fureby, On the supersonic flame structure in the HyShot II scramjet combustor, in: 26th ICDERS, Boston, USA, 2017.

[122] T. Poinsot, D. Veynante, S. Candel, Quenching processes and premixed turbulent combustion diagrams, J. Fluid Mech. 228 (1991) 561–606.

[123] W. L. Roberts, J. F. Driscoll, M. C. Drake, L. P. Goss, Images of the quenching of a flame by a vortex - to quantify regimes of turbulent combustion, Combust. Flame 94 (1993) 58–69.

[124] A. W. Skiba, T. M. Wabel, C. D. Carter, S. D. Hammack, J. E. Temme, J. F. Driscoll, Premixed flames subjected to extreme levels of turbulence part I: Flame structure and a new measured regime diagram, Combust. Flame 189 (2018) 407–432.

[125] J. F. Driscol, J. H. Chen, A. W. Skiba, C. D. Carter, E. R. Hawkes, H. Wang, Premixed flames subjected to extreme turbulence: Some questions and recent answers, Prog. Energy Combust. Sci. 76 (2020) 100802.

[126] A. Y. Poludnenko, E. S. Oran, The interaction of high-speed turbulence with flames: Global properties and internal flame structure, Combust. Flame 157 (2010) 995–1011.

[127] A. Y. Poludnenko, E. S. Oran, The interaction of high-speed turbulence with flames: Turbulent flame speed, Combust. Flame 158 (2011) 301–326.

[128] A. J. Aspden, M. S. Day, J. B. Bell, Turbulence-flame interactions in lean premixed hydrogen: transition to the distributed burning regime, J. Fluid Mech. 680 (2011) 287–320.

[129] J. Savre, H. Carlsson, X. S. Bai, Tubulent methane/air premixed flame structure at high Karlovitz numbers, Flow Turbul. Combust. 90 (2013) 325–341.

[130] T. Nilsson, H. Carlsson, R. Yu, X. S. Bai, Structures of turbulent premixed flames in the high karlovitz number regime - DNS analysis, Fuel 216 (2018) 627–638.

[131] A. J. Aspden, M. S. Day, J. B. Bell, Towards the distributed burning regime in turbulent premixed flames, J. Fluid Mech. 871 (2019) 1–21.

[132] J. F. Driscoll, Premixed turbulent combustion regimes of thickened and distributed reactions, in: Proceedings of the 9th MCS, 2015.

[133] J. F. Driscoll, Premixed turbulent combustion in high Reynolds number regimes of thickened flamelets and distributed reactions, Tech. rep., Air Force Res. Lab. Report AFRL-AFOSR-VA-TR-2016-0136 (2016).

[134] A. Mura, V. A. Sabelnikov, Supersonic combustion, in: N. Swaminathan, X. S. Bai, N. E. L. Haugen, C. Fureby, G. Brethouwer (Eds.), Advanced Turbulent Combustion Physics and Applications, Cambridge University Press (2021, to appear).

[135] E. S. Shchetinkov, Calculation of flame velocity in turbulent stream, Symp. (Int.) Combust. 7 (1958) 583–589.

[136] E. S. Shchetinkov, Physics of Gases Combustion, Nauka (Science), Moscow (in russian), 1965.

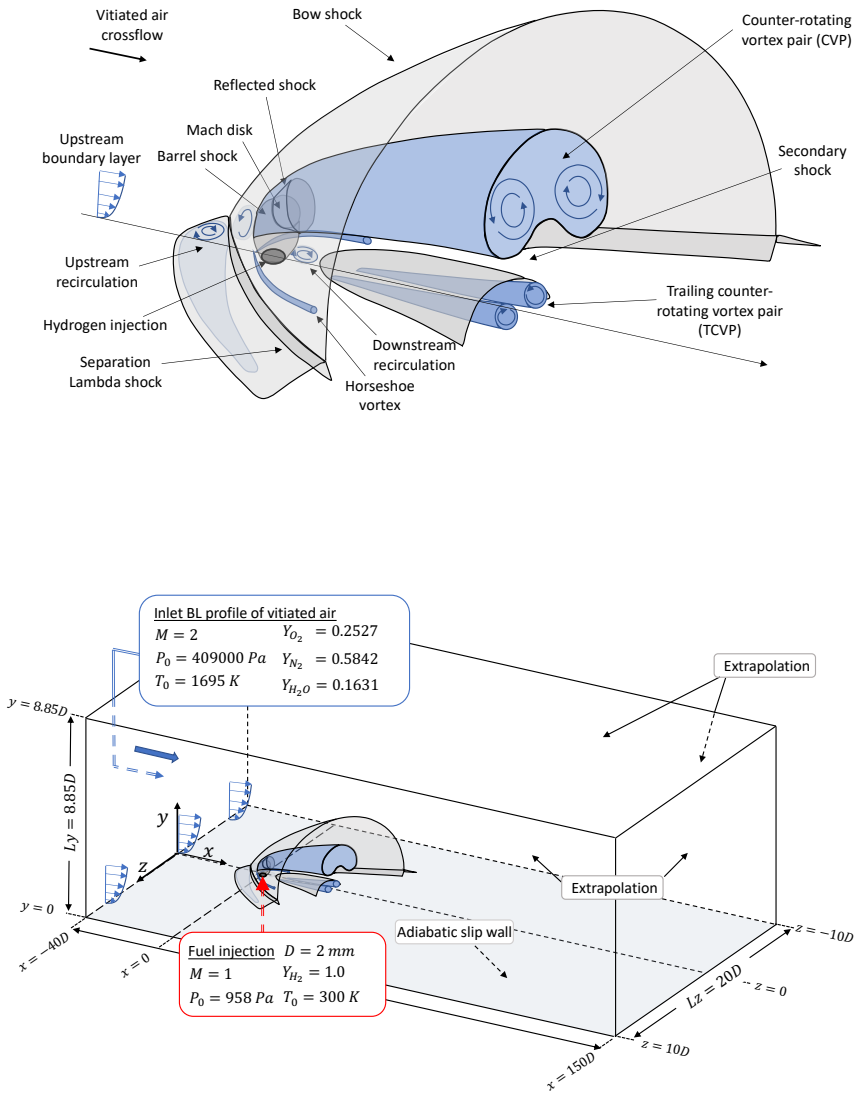

Fig. 1. Top: three-dimensional schematic view of the flow topology of the underexpanded jet in supersonic crossflow (JISCF). Bottom: definition of the computational domain and associated boundary conditions.

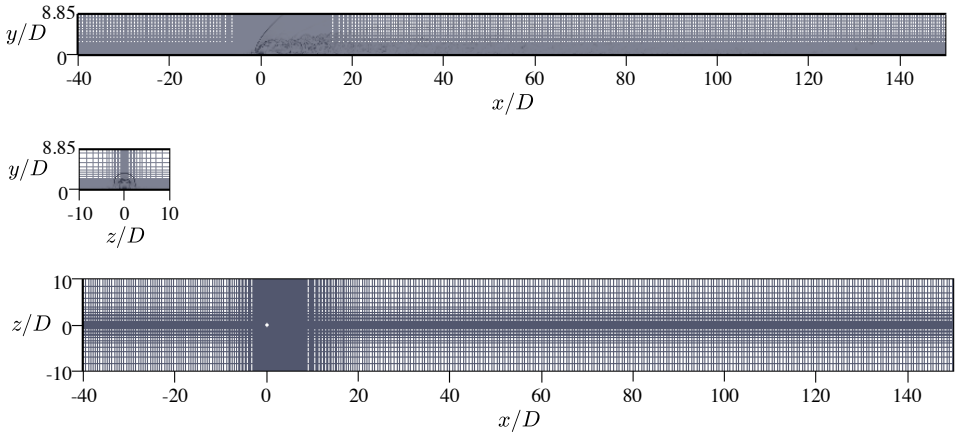

Fig. 2. Computational mesh overview (one single line depicted for six successive nodes).

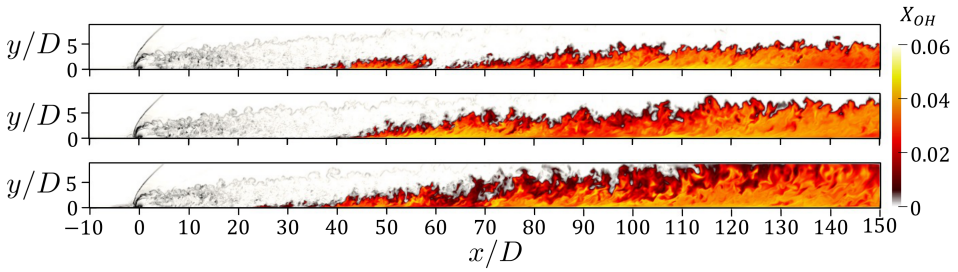

Fig. 3. Temporal evolution in the median plane $z/D = 0.0$ of the molar fraction of hydroxyl radical displayed together with a numerical Schlieren, from top to bottom, $t^* = 80.0$, 100.0, and 170.0.

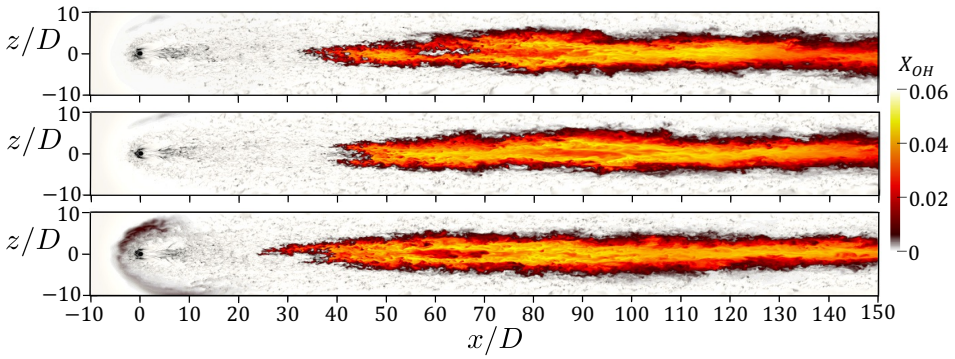

Fig. 4. Temporal evolution in the median plane $y/D = 0.25$ of the molar fraction of hydroxyl radical displayed together with a numerical Schlieren, from top to bottom, $t^* = 80.0$, 100.0, and 170.0.

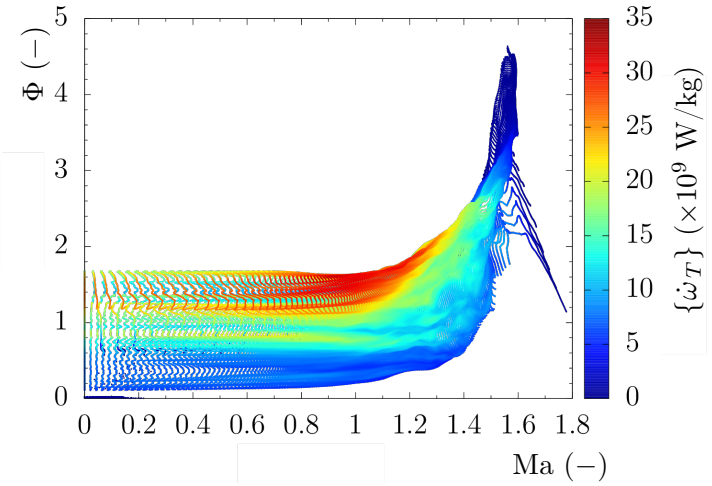

Fig. 5. Distribution of the combustion regime (subsonic / supersonic) evaluated in conditions featuring a HRR value that exceeds one percent of its maximal value $\dot{\omega}_{T,\max}$. The equivalence ratio is plotted versus the Mach number and the distribution is colored by the averaged HRR.

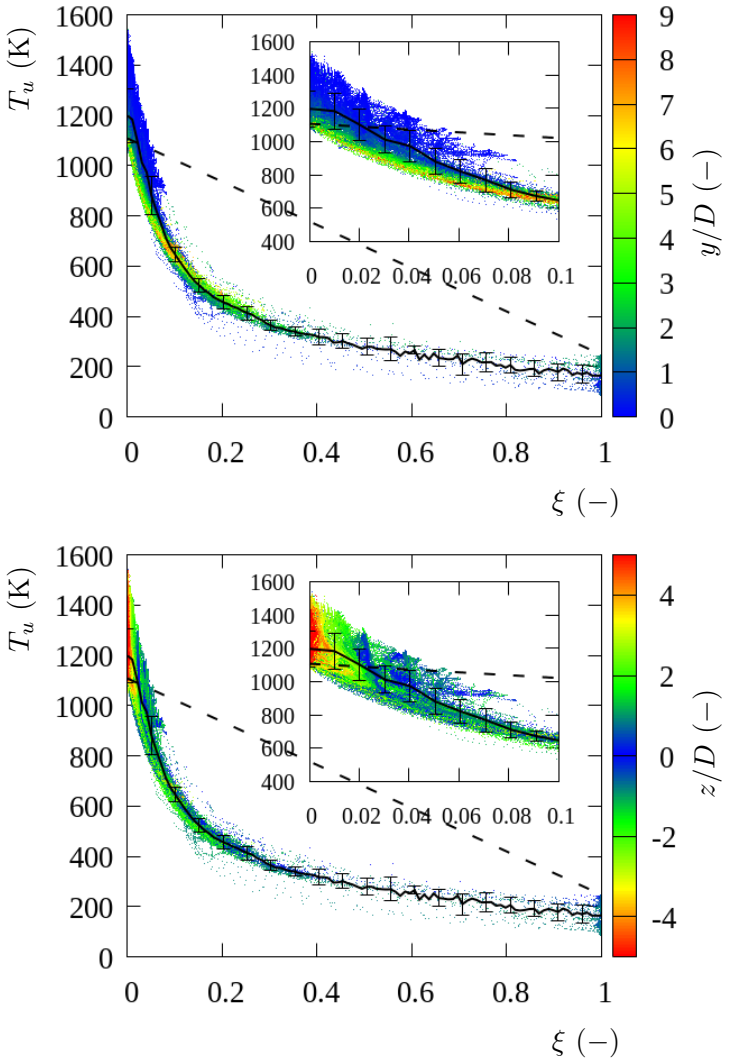

Fig. 6. Scatterplots of the unburnt mixture temperature obtained at $t = t_i = 150.0D/u_\infty$ plotted versus the mixture fraction as extracted from planes $x/D = 0.0$, 25.0, 50.0, and 100.0 together with the corresponding conditional average (continuous black line) and with the linear approximation (black dashed line). The dots are colored by normalized coordinates y/D (top) and z/D (bottom).

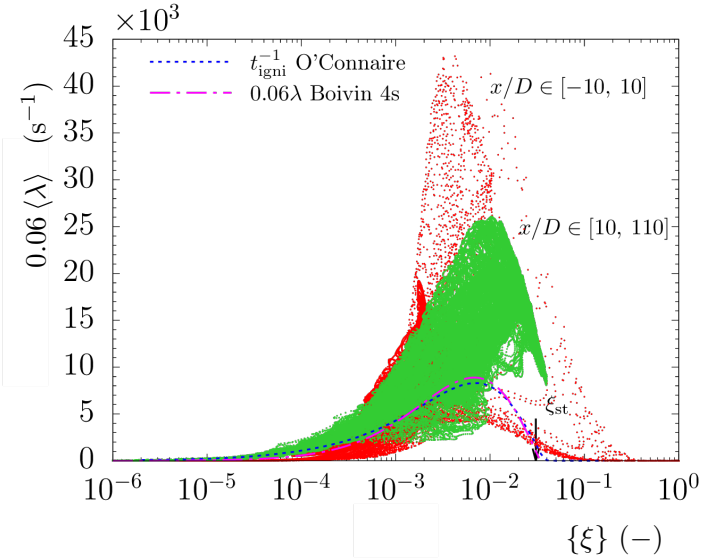

Fig. 7. Scatterplots of the reactivity λ plotted versus the mixture fraction in the direct vicinity of the injection ($-10.0 < x/D < 10.0$; red dots) and downstream of the injection ($10.0 < x/D < 110.0$; green dots). Comparison between PSR computations of *(i)* the ignition delay using the chemical scheme of Ó Connaire *et al.* [102] (dashed line) and *(ii)* reactivity λ using the reduced chemistry of Boivin *et al.* [100].

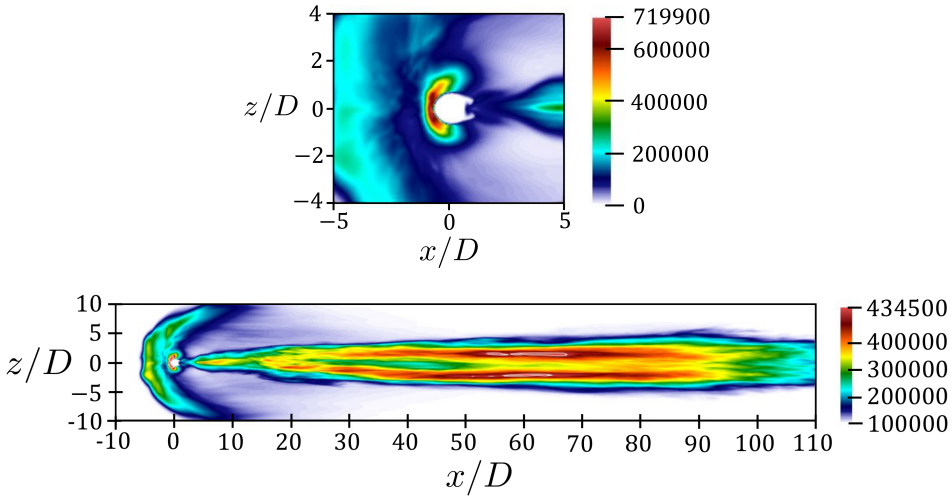

Fig. 8. Parietal field of the averaged reactivity $\langle\lambda\rangle$ (s^{-1}). Zoom on the injection (top) and general view (bottom). The isoline $0.95\,\langle\lambda\rangle_{max}$ is depicted with a white line.

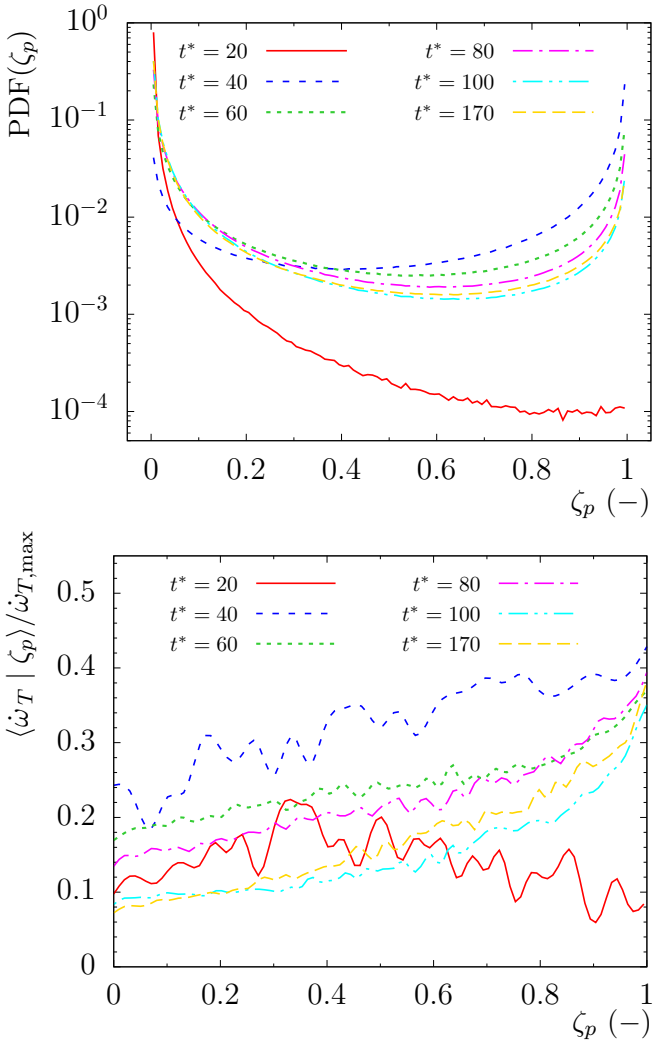

Fig. 9. Analysis of the non-premixed and premixed modes contributions evaluated in computational cells featuring a HRR value that exceeds one percent of its maximal value $\dot{\omega}_{T,\max}$ at times $t^* = 20.0$, 40.0, 60.0, 80.0, 100.0, and 170.0. Top: probability density function (PDF) of the premixedness index. Bottom: conditional average of the normalized HRR plotted versus the premixedness index.

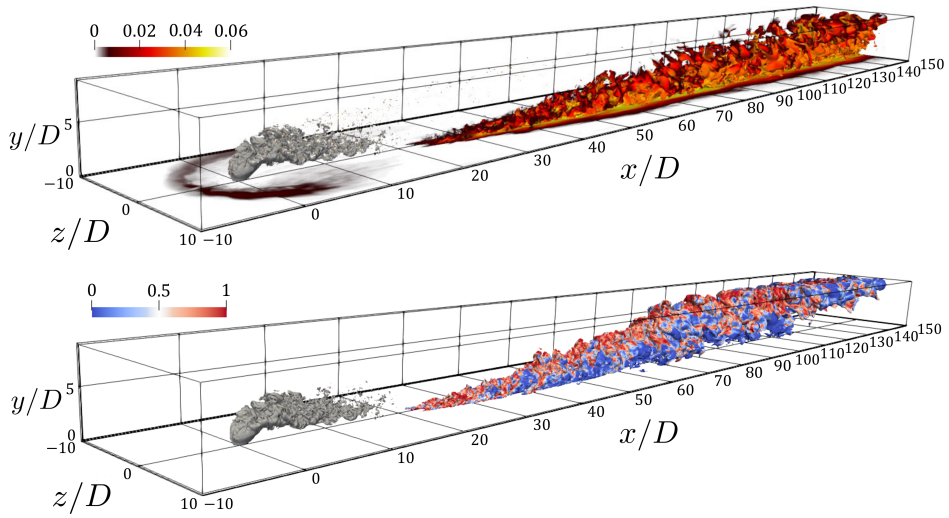

Fig. 10. Instantaneous flame structure at $t^* = 170.0$. Top: iso-surface of the stoichiometric mixture fraction colored by the OH molar fraction and parietal field of the same quantity. Bottom: iso-surface of the stoichiometric mixture fraction colored by the premixedness index. The grey iso-surface corresponds to the mixture fraction $\xi = 0.5$.

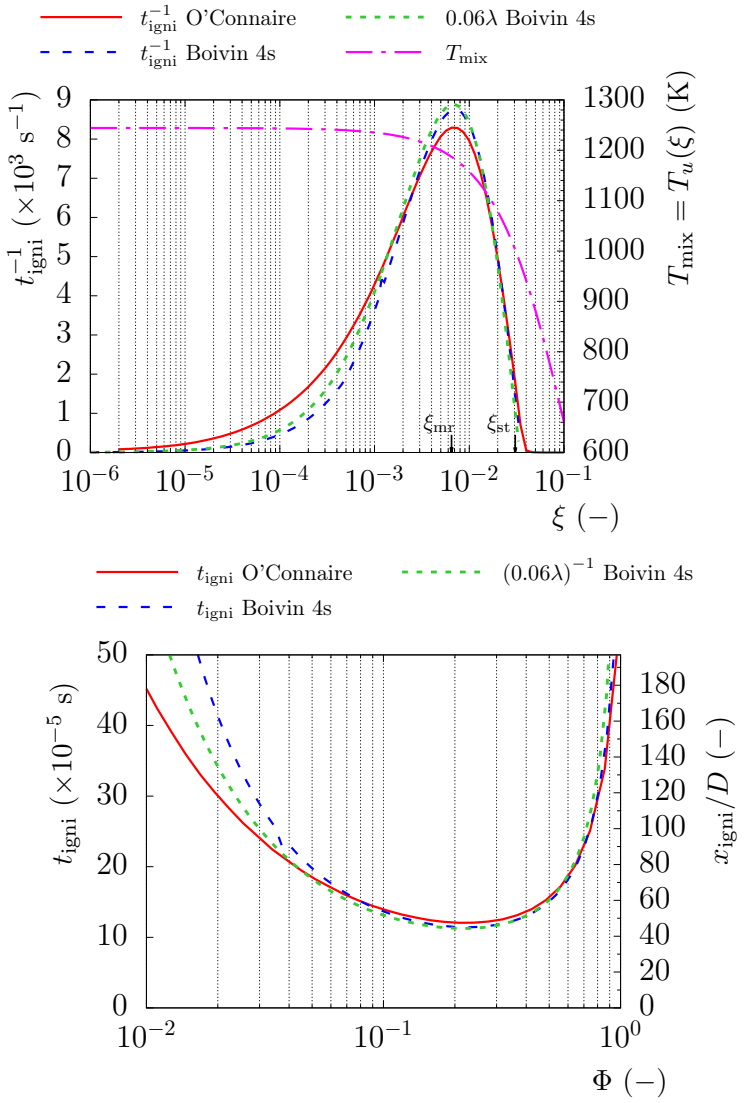

Fig. 11. Ignition delay time t_{igni} plotted versus the mixture fraction ξ (top) and equivalence ratio Φ (bottom) with a range of variation equivalent to $\xi \in \left[3.0 \cdot 10^{-4}, \xi_{\text{st}}\right]$. Comparison between the results obtained with the detailed mechanism of Ó Connaire *et al.* [102], the reduced mechanism of Boivin *et al.* [100], and the reactivity λ, which is obtained at the initial time of computation. The estimate of the combustion stabilization abscissa is deduced from $x_{\text{igni}} = 0.6 u_\infty t_{\text{igni}}$.

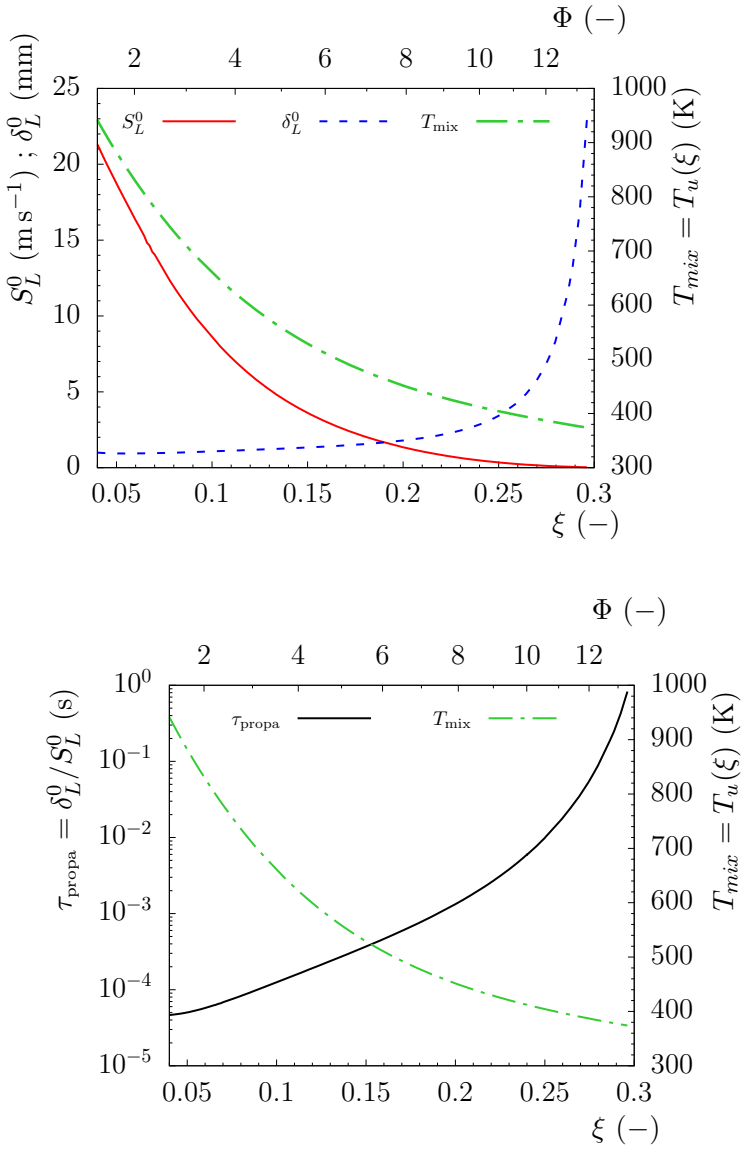

Fig. 12. Laminar flame velocity S_L^0 and thickness δ_L^0 (top) and flame transit time δ_L^0/S_L^0 (bottom) as a function of the mixture fraction ξ (and global equivalence ratio Φ). Computations performed with the detailed mechanism of Jachimowski *et al.* [110].

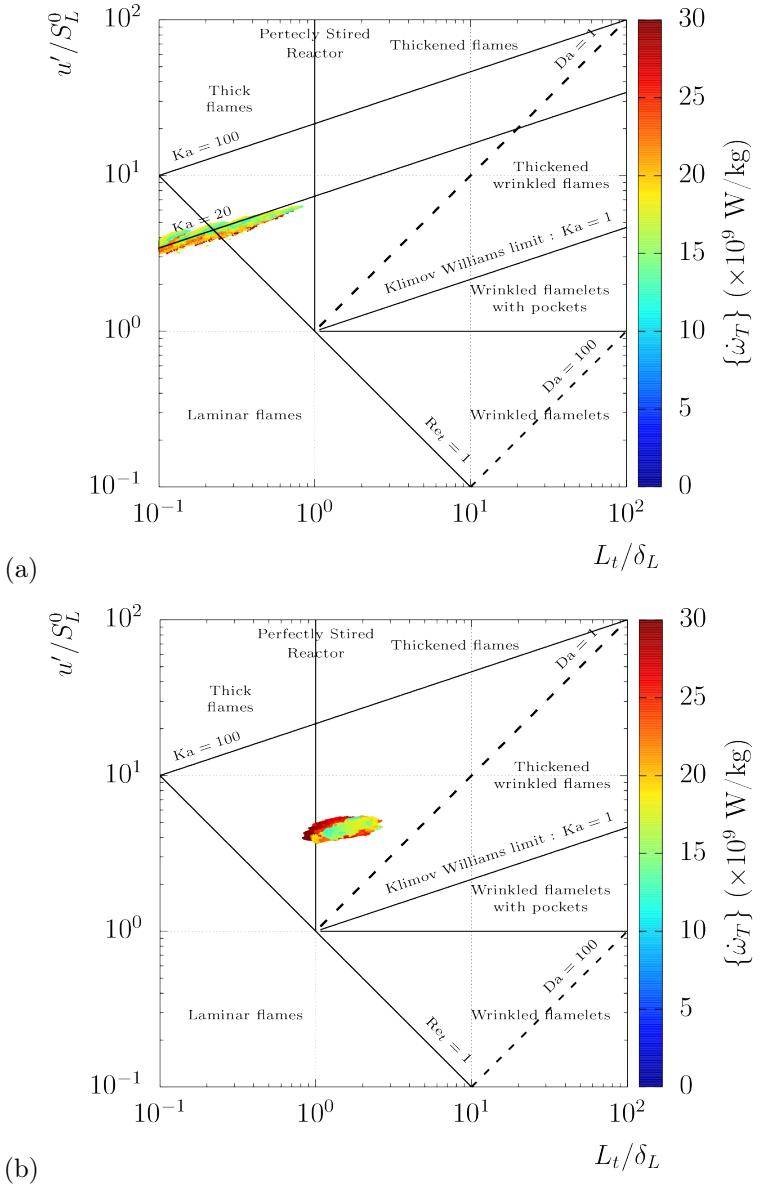

Fig. 13. Combustion regime scatterplots in the Barrère-Borghi coordinates. Data are collected in plane $y/D = 0.0$ (Fig. 13(a)), in plane $y/D = 0.25$ (Fig. 13(b)), in the longitudinal median plane $z/D = 0.0$ (Fig. 13(c)), and in cross-stream planes $x/D = 25.0$, 50.0, 75.0, 100.0, and 125.0 (Fig. 13(d)). Dots are colored by the heat release rate.

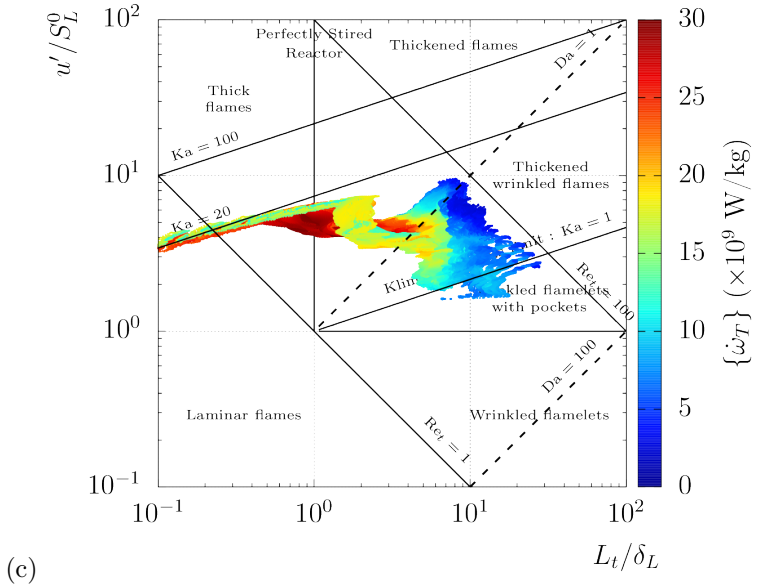

(c)

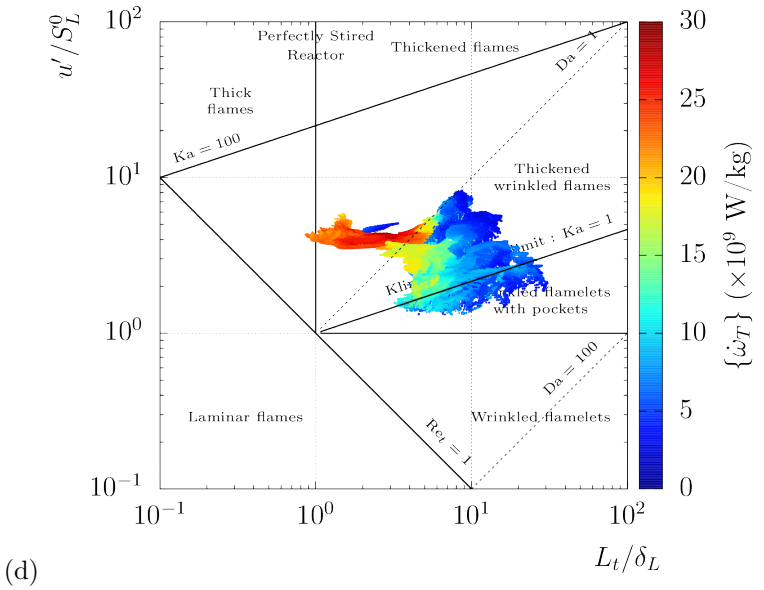

(d)

Fig. 13. Cont'd.

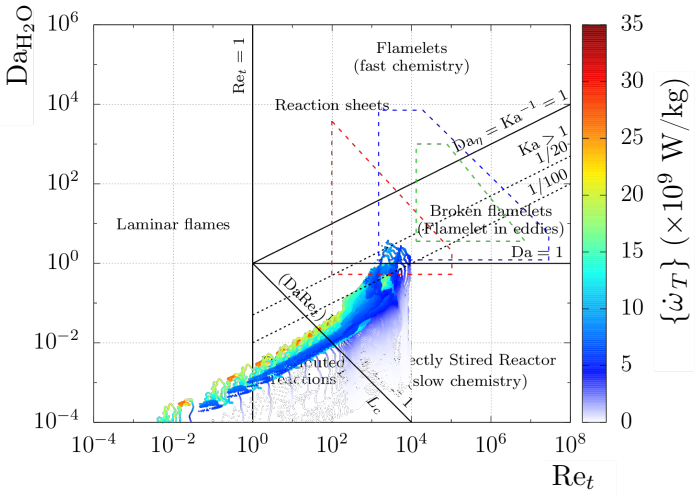

Fig. 14. Turbulent combustion diagram $(\mathrm{Re}_t, \mathrm{Da}_{\mathrm{H_2O}})$ with a chemical time scale deduced from the water vapor production rate. Data are collected in the median plane ($z/D = 0.0$). Dots are colored by the heat release rate. The red frame corresponds to the supersonic combustion regimed defined by Ingenito and Bruno [76]. The blue and green frames stand for the possible and most probable domains introduced by Balakrishnan and Williams [75].

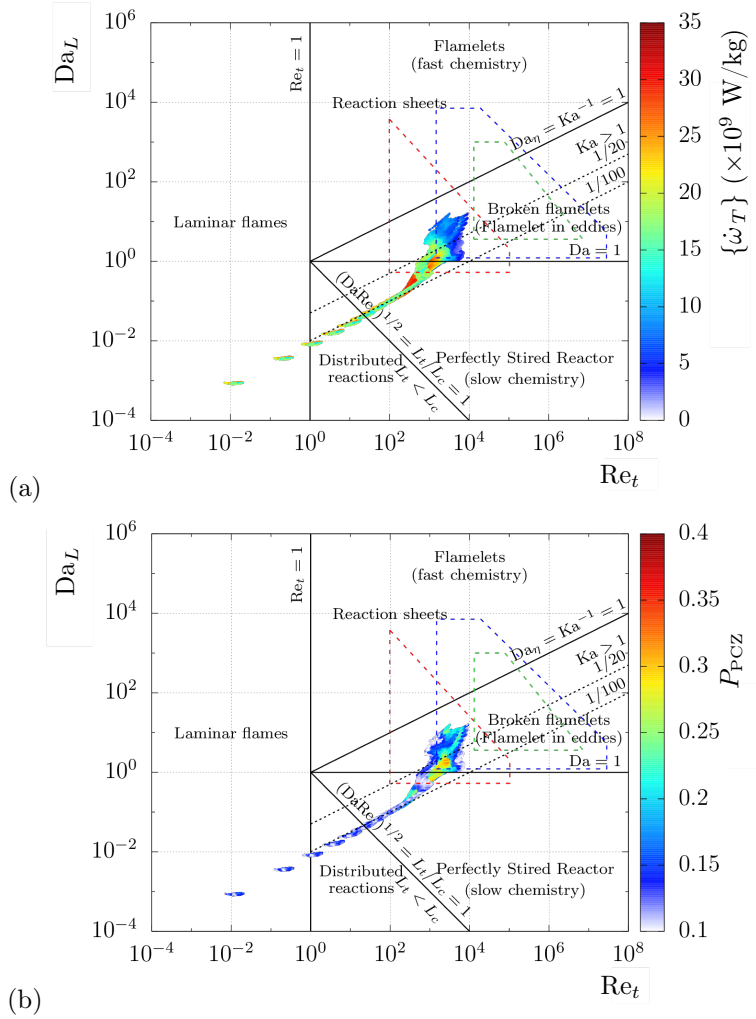

Fig. 15. Turbulent combustion diagrams (Re_t,Da_L) with a chemical time scale deduced from the laminar premixed flame transit time δ_L^0/S_L^0. Data are collected in the median plane ($z/D = 0.0$). Dots are colored by *(i)* the heat release rate (Fig. 15(a)), *(ii)* probability that the premixedness index exceeds 0.7 (Fig. 15(b)), *(iii)* Mach number Ma (Fig. 15(c)), *(iv)* turbulent Mach number Ma_t (Fig. 15(d))), *(v)* normalized streamwise coordinate x/D (Fig. 15(e)), and *(vi)* normalized wall-normal coordinate y/D (Fig. 15(f)).

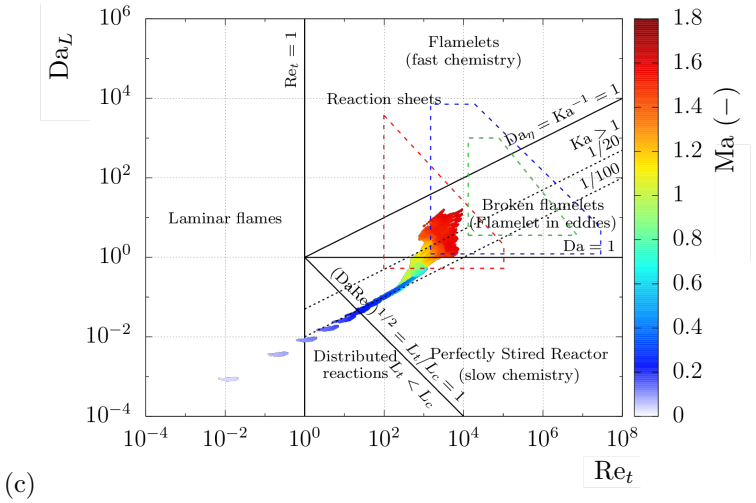

(c)

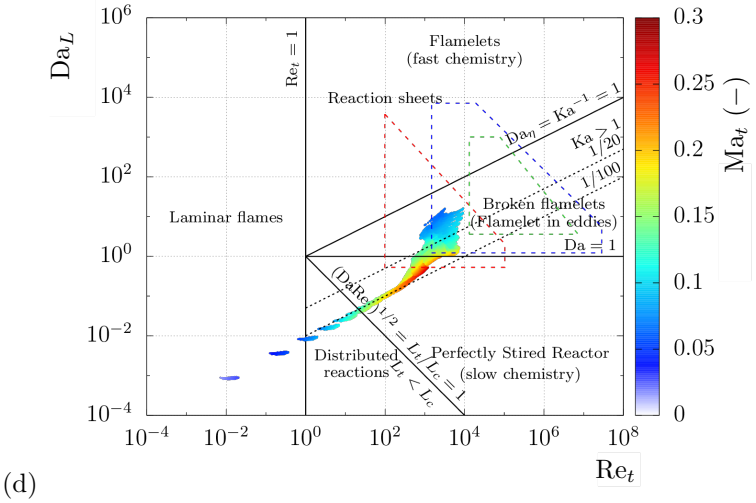

(d)

Fig. 15. Cont'd.

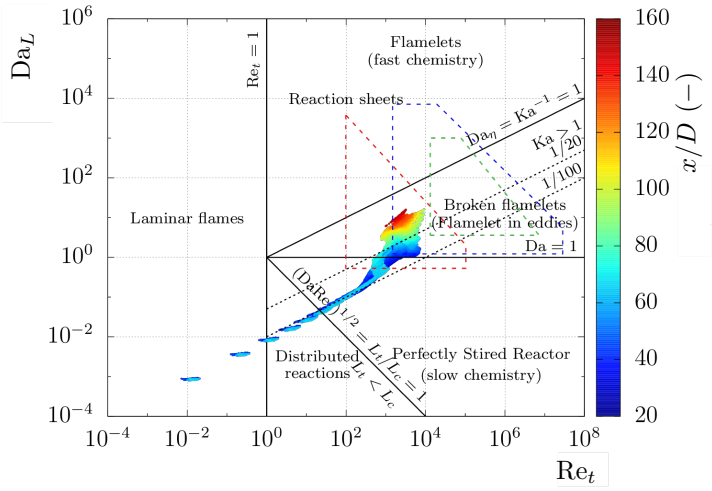

(e)

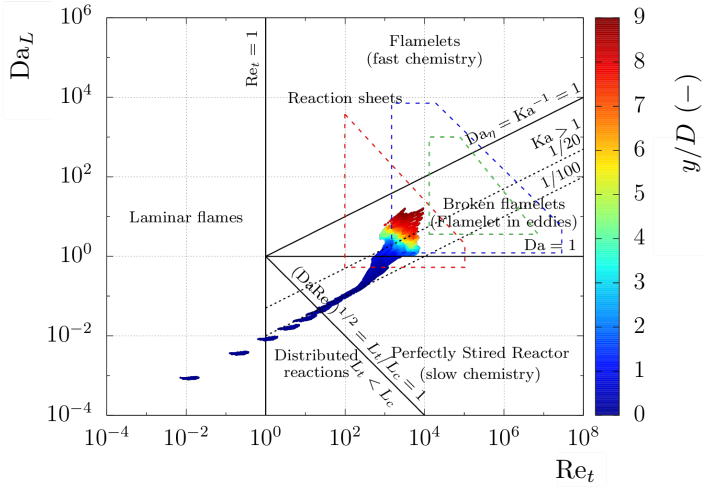

(f)

Fig. 15. Cont'd.

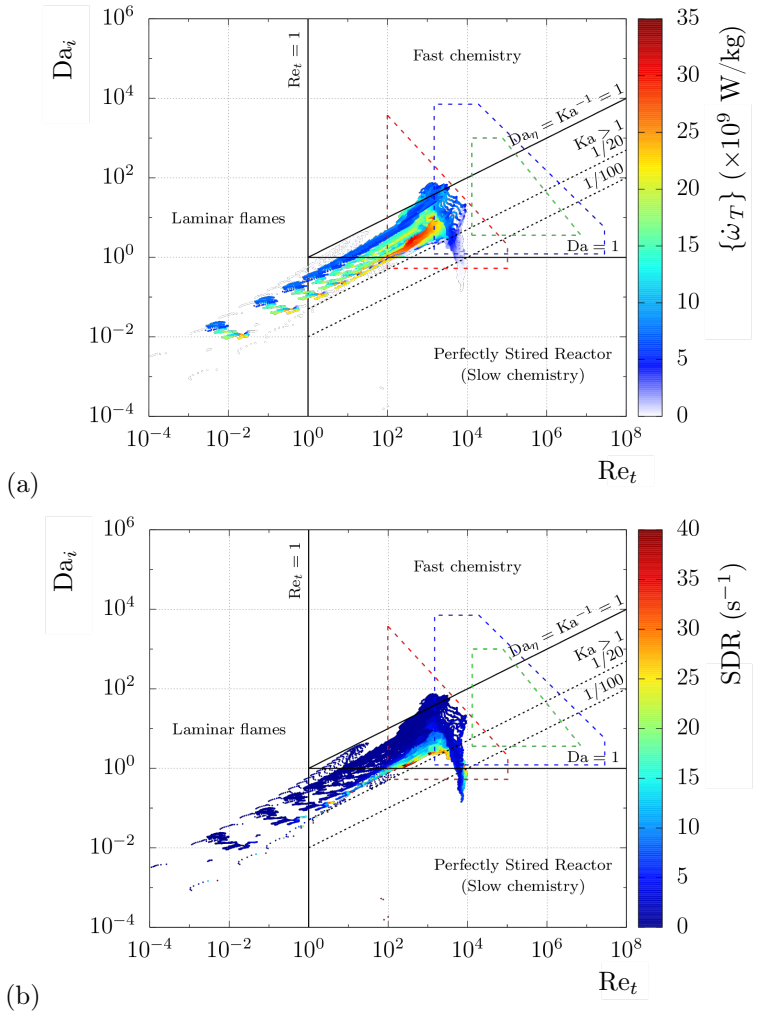

Fig. 16. Turbulent combustion diagrams (Re_t,Da_i) with a chemical time scale deduced from the reactivity λ. Data are collected in the median plane ($z/D = 0.0$). Dots are colored by *(i)* the heat release rate (Fig. 16(a)), *(ii)* the SDR (Fig. 16(b)), *(iii)* Mach number Ma (Fig. 16(c)), *(iv)* turbulent Mach number Ma_t (Fig. 16(d))), *(v)* normalized streamwise coordinate x/D (Fig. 16(e)), and *(vi)* normalized wall-normal coordinate y/D (Fig. 16(f)).

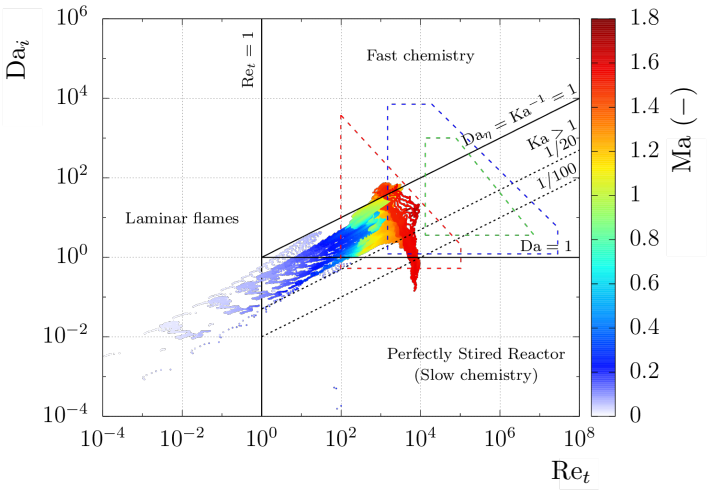

(c)

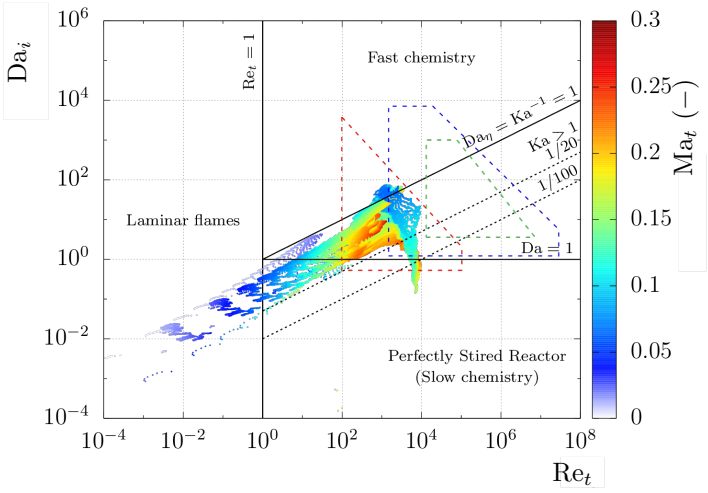

(d)

Fig. 16. Cont'd.

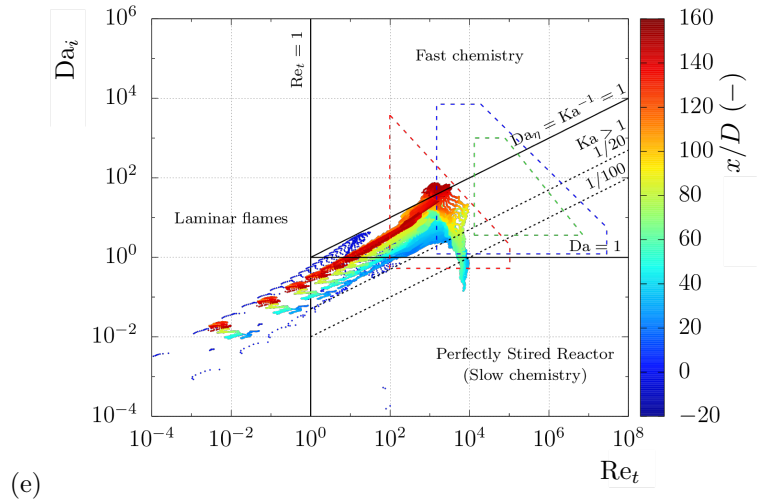

(e)

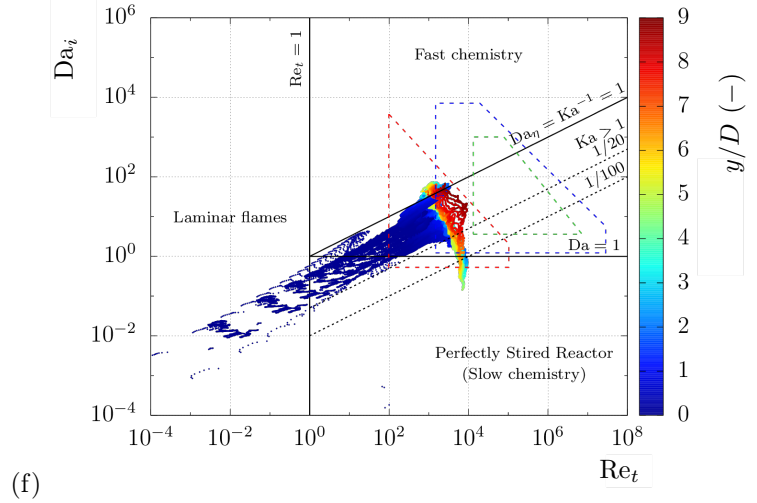

(f)

Fig. 16. Cont'd.